Fundamental Study on Crystal Growths of Metal Oxides within Confined Spaces

亀井, 龍真

Fundamental Study on Crystal Growths of Metal Oxides within Confined Spaces

（閉鎖空間内における金属酸化物結晶成長法に関する基礎的研究）

Ryoma Kamei

Ph.D. Thesis **September 2023**

Fundamental Study on Crystal Growths of Metal Oxides within Confined Spaces

A Dissertation Submitted to

Interdisciplinary Graduate School of Engineering Science
Kyushu University

by

Ryoma Kamei

In Partial Fulfilment of the Requirements for the Degree of

Doctor of Philosophy in Engineering

September 2023

Abstract

Unlike an open environment, crystal growth in an enclosed space improves interactions with molecules, enabling highly efficient separation and recovery of molecules. Taking advantage of its characteristics, it is applied in various fields such as organic modification, MOF, and microfluidics. Crystal growth into confined spaces has mainly been done with organic materials. However, organic substances are known to be weak against heat because they are generally covalent bonds. Therefore, we focused on metal oxides, which are inorganic materials. Metal oxides are known to have excellent heat resistance due to ionic bonding. Crystal growth of metal oxides in confined spaces has been done in the past by various methods such as hydrothermal synthesis, ALD and sol-gel. However, it has been found that there is no report of crystal growth at a certain region when metal oxide crystal growth is performed in a closed space by the conventional method. Therefore, in this paper, we try hydrothermal synthesis, which is a crystal growth method for metal oxides, and investigate the cause of poor crystal growth by coating ALD in a closed space. Metal oxide crystal growth is performed in a closed space in a region that could not be reached before.

ZnO nanowires were prepared by hydrothermal synthesis for the modification of nanostructures to microtubes. This method was adopted because the procedure is very simple and excellent in safety. Two steps are required to modify the inner wall of microtubes with ZnO nanowires by hydrothermal synthesis. First, ZnO seed layer for nanowire growth is formed on

the entire inner wall of the tube. Next, hot solution is supplied into the tube to grow ZnO nanowires. In conventional hydrothermal synthesis no grow ZnO nanowires at all in the case of microtubes with aspect ratios over 600. Conventional seed layer using zinc oxide forms a complex compound of Zn instead of ZnO inside the tube. Therefore, we solved this problem by supplying air to the inside of the tube when forming the seed layer to eliminate the impurities remaining inside the tube. As a result, we succeeded in growing uniform ZnO nanowires all over the inner wall of a microtube with an inner diameter of 100 μm, a length of 1 m, and an aspect ratio of 10,000.

ALD was applied to chemically modify the microtube, and a TiO_X film was created. ALD is a type of deposition method that enables film thickness control at the atomic layer level and enables uniform deposition even on structures. Although ALD is generally believed to be capable of uniformly depositing structures with poor conductance, it has been found that there are still areas that have not been achieved in terms of decoration in spaces with high aspect ratios, such as tubes. It is considered that the small diameter and long length of the tube deteriorates the conductance inside the tube, and the gas cannot be supplied in the conventional ALD. Therefore, we developed a new ALD that can forcibly supply gas even to a small-diameter long tube and created a recipe. The new ALD generates a forced gas flow by directly connecting a gas channel and a tube. Using this ALD, we created a recipe that gives a higher differential pressure (7000Pa or more) inside the tube than before and solved the problem. As

a result, we succeeded in forming a uniform TiO_X film on the entire inner wall of a microtube with an inner diameter of 100 μm, a length of 1 m, and an aspect ratio of 10,000.

Acknowledgment

This study was carried out at the Institute for Materials Chemistry and Engineering, and Department of Molecular and Material Sciences, Interdisciplinary Graduate School Engineering Sciences, Kyushu University during 2017-2022.

I am grateful to my supervisor, Prof. Takeshi Yanagida. Thanks to him, I learned the importance of scientific, logical thinking, the procedures of research, and the way how to express my thinking attractively.

I sincerely express my gratitude from the bottom of my heart to Assoc. Prof. Takuro Hosomi and Dr. Masaki Kanai for lots of his constant encouragement, invaluable discussions, constructive suggestions, and emotional support. I got the scientific knowledge, the frame of my mind for research, the interest in scientific research, thanks to him.

I really thank Assoc. Prof. Kazuki Nagashima for lots of his constant and strict encouragement and constructive suggestion. I learned the importance of scientific, logical thinking, and continuous study, thanks to him.

I sincerely express my gratitude from the bottom of my heart to Prof. Tsunaki Takahashi for lots of invaluable discussions and constructive suggestions. I got the scientific knowledge as to devices.

I deeply express my gratitude from the bottom of my heart to Assis. Prof. Wataru Tanaka for discussion on organic chemistry. I would like to thank Dr. Eisuke Kanao, Prof Takuya Kubo

and Mr. Katsuya Nakano for technical support as to PHLC analysis.

Mainly, I would like to thank Dr. Benjarong Samransuksamer for their support and stimulating discussions. I would like to thank Ms. Hiroko Imaizumi for their daily support. I would like to thank all students in Yanagida Lab. in IMCE Kyushu University: Ms. Xixi Zhao, Dr. Jiangyang Liu, Ms. Wenjun Li, Mr. Chaiyanut Jirayupat and Mr. Kentaro Nakamura. And in University of Tokyo: Mr. Haruka Honda, Mr. Shumpei Kurose, Mr. Yusuke Tonomoto, Mr. Shintaro Nagata, Mr. Yu Yamaguchi, Mr. Motoki Date, Mr. Wenjin Lei, Mr. Haruya Endo, Mr. Takeshi Ono, Mr. Hiroki Dan and Mr. Kosuke Yamaoka.

I acknowledge all alumni of Yanagida Lab: Dr. Guozhu Zhang, Dr. Chen Wang, Dr. Zetao Zhu, Dr. Hiroshi Anzai, Dr. Hao Zeng, Dr. Ruolin Yan, Mr. Satoru Shiraishi, Mr. Masahiro Shimizu, Mr. Mizuki Matsui, Mr. Shojiro Hayata and Mr. Rimon Yamaguchi for their constant encouragement and constructive discussions.

I would like to thank my family for their support and understanding of my study. I thank my friends for their support. Finally, I thank all encounters with the kind people during my Ph.D. course.

Ryoma Kamei

Table of Contents

Chapter I

General Introduction

1.1 General Introduction

1.1.1 Chemical approach to confined spaces

Altering the surface structure within the confined space can alter interactions with molecules. Therefore, specific molecules with strong surface properties and interactions can be separated and collected. In recent years, utilizing this surface property, research has been conducted in various closed spaces such as organic catalysts[1,2] , MOFs[3,4] , and microchannels[5,6] . Organic materials are easy to design, but they are generally said to be weak against heat because the bonds between molecules are covalent bonds. Therefore, we focused on metal oxides with excellent heat resistance. However, a search of past literature reveals that there are limits to conventional metal oxide crystal growth in closed spaces[7-9] . In this paper, we grow metal oxide crystals in microtubes, which are closed spaces. By investigating the chemical factors that inhibit crystal growth and solving the problems, we will realize metal oxide crystal growth in a closed space region, which was not possible until now.

Molecular separations using capillary tubes and microfluidic, which are widely used, are based on the interaction of molecules with solid surfaces in confined spaces. In order to control this interaction, it is effective to modify or change the surface structure and surface properties.[10-13] By changing the structure and physical properties of the surface, it is possible to change the interaction with molecules by changing the ionic structure. Effectively utilizing

the interaction with molecules in this way, it may be possible to provide molecular separation and new organic synthesis methods that could not be realized so far. However, in order to make effective use of interactions with molecules, it is currently believed that a thin and long structure with a large surface area-to-volume ratio is effective. Reports of such structural and chemical modifications are limited.[14-17]

1.1.2 Metal oxide crystal growth in confined space

Crystal growth of metal oxides in confined spaces can modify the surface structure, and its high thermal robustness may enable highly reproducible collection and separation of molecules. However, reports on the growth of metal oxide crystals in confined spaces are currently limited. In other words, there are no restrictions on crystal growth of metal oxides in open systems, but crystal growth may not occur in closed spaces due to some restrictions. Solving this problem opens up new possibilities for growing metal oxide crystals in confined spaces, which could make a significant contribution to the field of molecular trapping and separation.

At present, reports on structural and chemical modifications to the interior of small-diameter and long structures are predominantly based on liquid-phase deposition.[18-20] Monolith columns are common for liquid phase-based nanostructures.[21,22] Monolithic column can create a lot of structure on the inner wall of the tube, but the surface area is too large and a large force must be applied to feed the molecules. As a result, less stable molecules may be degraded and the desired molecule may not come out. Nanostructures in monolithic columns are difficult to control because they are deposited by a sol-gel method. On the other hand, liquid phase chemical modification can easily chemically modify thin and long structures, but there are problems with film thickness control and reproducibility. Structural and chemical modifications to the inside of the elongated structure are thought to be the cause of the difficulty in supplying and discharging natural gas due to a decrease in conductance. For this reason, it

is difficult to grow a structure that causes a chemical reaction inside the tube or to chemically modify the tube using gas.

1.1.3 ZnO nanowire crystal growth in confined space

In this paper, as a structural modification approach, we created ZnO nanowires that can be grown by immersion in liquid phase under high temperature called hydrothermal synthesis.[23-25]Hydrothermal synthesis is a technique that deposits a material called a seed layer on the surface of a sample on which nanostructures are to be grown and grows nanostructures from sample. However, at the beginning of the experiment, it was not possible to grow the nanostructure uniformly inside the long thin structure. The reason for this is considered to be that the ZnO seed layer could not be formed because the impurities could not be removed when the seed layer was formed because the sample had a long structure with a small diameter. Therefore, the ZnO seed layer was deposited by forcibly removing the impurities by forcibly blowing air during the formation of the seed layer. As a result, we succeeded in growing nanostructures uniformly in a long tube with an inner diameter of 100μm, a length of 1m and an aspect ratio of 10,000.

1.1.4 Metal oxide modification to confined space

The chemical modification approach was ALD. ALD is a type of CVD that enables film thickness control at the atomic layer level, and is a suitable growth method for uniform growth

of high-aspect spaces and structures[26-29]However, when we actually performed ALD film formation, it became clear that there was a limit to the modification. This is because ALD instruments usually change the shape of the sample by placing it in a chamber, so the smaller inner diameter of the tube and the longer the tube, the lower the conductance, leaving most of the gas in the chamber outside the tube for it to flow. Therefore, we developed a device that can directly connect the gas flow path and the tube and created a deposition recipe that can be used for small diameter and long tubes. The device developed this time can generate a differential pressure in the tube that cannot be obtained with normal ALD, so it can generate a forced flow in the tube. Using this new ALD method, we succeeded in uniformly chemically modifying the inside of a long tube with an inner diameter of 100μ, a length of 1m, and an aspect ratio of 10,000.

1.1.5 The Objective and the Structure of This Thesis

This book consists of 6 chapters. Chapter 2 provides an overview of previous research on structural and chemical modification into confined spaces. Chapter 3 details a previously unattainable method for growing inorganic nanostructures on the inner walls of capillary tubes with aspect ratios greater than 10,000. Next, in Chapter 4, we describe a method for separating AMP, ADP, and ATP, which have been difficult to separate, using inorganic nanostructures grown on the inner walls of capillaries. And in Chapter 5, we will explain the equipment outline

and growth method for performing ALD in a confined space that has not been realized so far.

Finally, Chapter 6 concludes with a summary of the overall content of the book.

1.2 References

[1] Wayner, Danial D. M., and Robert A. Wolkow. 2002. "Organic Modification of Hydrogen Terminated Silicon Surfaces 1." *Journal of the Chemical Society, Perkin Transactions 2* 0 (1): 23–34.

[2] Das, Amit, Francis Reny Costa, Udo Wagenknecht, and Gert Heinrich. 2008. "Nanocomposites Based on Chloroprene Rubber: Effect of Chemical Nature and Organic Modification of Nanoclay on the Vulcanizate Properties." *European Polymer Journal* 44 (11): 3456–65.

[3] Shekhah, O., J. Liu, R. A. Fischer, and Ch Wöll. 2011. "MOF Thin Films: Existing and Future Applications." *Chemical Society Reviews* 40 (2): 1081–1106.

[4] Pan, Congjie, Weifeng Wang, Huige Zhang, Laifang Xu, and Xingguo Chen. 2015. "In Situ Synthesis of Homochiral Metal–organic Framework in Capillary Column for Capillary Electrochromatography Enantioseparation." *Journal of Chromatography. A* 1388 (April): 207–16.

[5] Rahong, Sakon, Takao Yasui, Takeshi Yanagida, Kazuki Nagashima, Masaki Kanai, Gang Meng, Yong He, et al. 2015. "Three-Dimensional Nanowire Structures for Ultra-Fast Separation of DNA, Protein and RNA Molecules." *Scientific Reports* 5 (June): 10584.

[6] Yasui, Takao, Takeshi Yanagida, Satoru Ito, Yuki Konakade, Daiki Takeshita, Tsuyoshi Naganawa, Kazuki Nagashima, et al. 2017. "Unveiling Massive Numbers of Cancer-Related Urinary-microRNA Candidates via Nanowires." *Science Advances* 3 (12): e1701133.

[7] Cremers, Véronique, Riikka L. Puurunen, and Jolien Dendooven. 2019. "Conformality in Atomic Layer Deposition: Current Status Overview of Analysis and Modelling." *Applied Physics Reviews* 6 (2): 021302.

[8] Nolan, Mark, Ian Povey, Simon Elliot, Nicolas Cordero, Martyn Pemble, Brian Shortt, and

Marcos Bavdaz. 2012. “Uniform Coating of High Aspect Ratio Surfaces through Atomic Layer Deposition.” In *Space Telescopes and Instrumentation 2012: Ultraviolet to Gamma Ray*, 8443:1086–93. SPIE.

[9] Becker, Jill S., Seigi Suh, Shenglong Wang, and Roy G. Gordon. 2003. “Highly Conformal Thin Films of Tungsten Nitride Prepared by Atomic Layer Deposition from a Novel Precursor.” *Chemistry of Materials: A Publication of the American Chemical Society* 15 (15): 2969–76.

[10] Hosoya, Ken, Natsuki Hira, Katsuya Yamamoto, Masaru Nishimura, and Nobuo Tanaka. 2006. “High-Performance Polymer-Based Monolithic Capillary Column.” *Analytical Chemistry* 78 (16): 5729–35.

[11] Pan, Congjie, Weifeng Wang, Huige Zhang, Laifang Xu, and Xingguo Chen. 2015. “In Situ Synthesis of Homochiral Metal–organic Framework in Capillary Column for Capillary Electrochromatography Enantioseparation.” *Journal of Chromatography. A* 1388 (April): 207–16.

[12] Suwatthanarak, Thanawat, Ivan Adiyasa Thiodorus, Masayoshi Tanaka, Taisuke Shimada, Daiki Takeshita, Takao Yasui, Yoshinobu Baba, and Mina Okochi. 2021. “Microfluidic-Based Capture and Release of Cancer-Derived Exosomes via Peptide–nanowire Hybrid Interface.” *Lab on a Chip* 21 (3): 597–607.

[13] Becker, Jill S., Seigi Suh, Shenglong Wang, and Roy G. Gordon. 2003. “Highly Conformal Thin Films of Tungsten Nitride Prepared by Atomic Layer Deposition from a Novel Precursor.” *Chemistry of Materials: A Publication of the American Chemical Society* 15 (15): 2969–76.

[14] Nolan, Mark, Ian Povey, Simon Elliot, Nicolas Cordero, Martyn Pemble, Brian Shortt, and Marcos Bavdaz. 2012. “Uniform Coating of High Aspect Ratio Surfaces through Atomic Layer Deposition.” In *Space Telescopes and Instrumentation 2012: Ultraviolet to Gamma Ray*, 8443:1086–93. SPIE.

[15] Gong, Ting, Longfei Hui, Jianwei Zhang, Daoan Sun, Lijun Qin, Yongmei Du, Chunying Li, Jian Lu, Shenlin Hu, and Hao Feng. 2015. "Atomic Layer Deposition of Alumina Passivation Layers in High-Aspect-Ratio Tubular Reactors for Coke Suppression during Thermal Cracking of Hydrocarbon Fuels." *Industrial & Engineering Chemistry Research* 54 (15): 3746–53.

[16] Mishra, Mrinalini, Chi-Chung Kei, Yu-Hsuan Yu, Wei-Szu Liu, and Tsong-Pyng Perng. 2017. "Uniform Coating of Ta2O5 on Vertically Aligned Substrate: A Prelude to Forced Flow Atomic Layer Deposition." *The Review of Scientific Instruments* 88 (6): 065103.

[17] Bigham, Shaun, Jennifer Medlar, Abuzar Kabir, Chetan Shende, Abdel Alli, and Abdul Malik. 2002. "Sol- Gel Capillary Microextraction." *Analytical Chemistry* 74 (4): 752–61.

[18] Pan, Congjie, Weifeng Wang, Huige Zhang, Laifang Xu, and Xingguo Chen. 2015. "In Situ Synthesis of Homochiral Metal–organic Framework in Capillary Column for Capillary Electrochromatography Enantioseparation." *Journal of Chromatography. A* 1388 (April): 207–16.

[19] Gu, Zhi-Yuan, Jun-Qing Jiang, and Xiu-Ping Yan. 2011. "Fabrication of Isoreticular Metal–Organic Framework Coated Capillary Columns for High-Resolution Gas Chromatographic Separation of Persistent Organic Pollutants." *Analytical Chemistry* 83 (13): 5093–5100.

[20] Hosoya, Ken, Natsuki Hira, Katsuya Yamamoto, Masaru Nishimura, and Nobuo Tanaka. 2006. "High-Performance Polymer-Based Monolithic Capillary Column." *Analytical Chemistry* 78 (16): 5729–35.

[21] Saito, Yoshihiro, Kiyokatsu Jinno, and Tyge Greibrokk. 2004. "Capillary Columns in Liquid Chromatography: Between Conventional Columns and Microchips." *Journal of Separation Science* 27 (17-18): 1379–90.

[22] Choi, Han-Seok, Mohammad Vaseem, Sang Gon Kim, Yeon-Ho Im, and Yoon-Bong Hahn. 2012. "Growth of High Aspect Ratio ZnO Nanorods by Solution Process: Effect of

Polyethyleneimine." *Journal of Solid State Chemistry* 189 (May): 25–31.

[23] Alenezi, Mohammad R., Simon J. Henley, and S. R. P. Silva. 2015. "On-Chip Fabrication of High Performance Nanostructured ZnO UV Detectors." *Scientific Reports* 5 (February): 8516.

[24] Greene, Lori E., Benjamin D. Yuhas, Matt Law, David Zitoun, and Peidong Yang. 2006. "Solution-Grown Zinc Oxide Nanowires." *Inorganic Chemistry* 45 (19): 7535–43.

[25] Knoops, Harm C. M., Stephen E. Potts, Ageeth A. Bol, and W. M. M. Kessels. n.d. "Atomic Layer Deposition." https://doi.org/10.1016/B978--444-63304-0.00027.

[26] Puurunen, Riikka L. 2005. "Surface Chemistry of Atomic Layer Deposition: A Case Study for the Trimethylaluminum/water Process." *Journal of Applied Physics* 97 (12): 121301.

[27] Leskelä, Markku, and Mikko Ritala. 2003. "Atomic Layer Deposition Chemistry: Recent Developments and Future Challenges." *Angewandte Chemie* 42 (45): 5548–54.

[28] George, Steven M. 2010. "Atomic Layer Deposition: An Overview." *Chemical Reviews* 110 (1): 111–31.

[29] Cremers, Véronique, Riikka L. Puurunen, and Jolien Dendooven. 2019. "Conformality in Atomic Layer Deposition: Current Status Overview of Analysis and Modelling." *Applied Physics Reviews* 6 (2): 021302.

Chapter II

Literature Reviews

2.1 Introduction

As described in chapter Ⅰ, the objective of this thesis is to investigate Uniform coating of metal oxide, an inorganic material, within narrow spatial regions previously unattainable. In Chapter 2, we will introduce research on chemical approaches to closed spaces that have been reported so far and deepen our understanding of chemical approaches to closed spaces.

As mentioned in Chapter 1, the goal of this paper is to chemically coat previously unattainable narrow spatial regions and exploit this property for new molecular separations. In Chapter 2, we will introduce research on chemical approaches to closed spaces that have been reported so far and deepen our understanding of chemical approaches to closed spaces.

- Section 2.2 summarizes organic modifications using confined spaces.
- Section 2.3 summarizes MOF using confined spaces.
- Section 2.4 summarizes microfluidic channels using confined spaces.
- Section 2.5 summarizes past metal oxide crystal growth in closed spaces.

2.2 Organic modifications using confined spaces

Organic modification can be easily modified by supplying a solution, and it is modified to metal oxide particles and capillary tubes such as confined spaces. Organic modifications are used in a wide range of applications in various fields, such as medicine[1,2], agriculture[3], optics[4,5], semiconductor devices[6-9] and catalysis[10,11]. This section mainly focuses on organic modifications to confined-space metal oxides.

2.2.1 Organic modification

Organic modification is a technology that can easily change the properties of surface materials by modifying organic substances into metal oxides.[1-6] The method of organic modification can be carried out mainly by supplying a solution containing any organic molecule to the metal oxide.[7-11] In other words, organic modification can easily change the surface properties of metal oxides, and these properties can be used to separate and recover molecules.

2.2.2 Organic modification to capillary tubes

Organic modifications into confined spaces such as capillary tubes have applications in molecular separation techniques such as GC-MS and LC-MS. Capillary tubes can separate various molecules such as hydrocarbons, alcohols, VOCs, pharmaceuticals, and aromatics by organically modifying Dimethylpolysiloxane, Diphenyl, Polyethylene Glycol, etc. This technique has been put into practical use and is used as a routine technique in chromatography. In recent years, organic modification of monolithic columns has also been investigated, and many studies have been conducted.[12-14]

Nanostructures modified into tubes and microchannels were mainly created to increase the

surface area of the channels and enhance their interaction with molecules. A classic example is monolithic columns, which are known to separate molecules faster and more efficiently than capillary columns. A monolith column was also used in previous publications to separate various molecules such as celiprolol, chlorpheniramine, etozoline, nomifensine, sulconazole, zopiclone, chlorpheniramine, tropicamide and warfarin.[1-8]However, due to the large surface area of this monolith column, it is necessary to push the molecules out with a stronger force than a normal capillary column. Therefore, weakly binding molecules may degrade during separation. The nanostructures used in microchannels then use nanowires grown by hydrothermal synthesis.[9-20]Nanowires can control the length and width of the nanostructures by the conditions of hydrothermal synthesis.[21,22]Microfluidic electrophoresis has been shown to separate DNA, protein, and RNA molecules faster than the electrical durability of capillaries. However, in past literature, nanostructures were prepared in an open state rather than directly modifying confined spaces.[9-20]That is, at present, there is no report of directly growing nanowires in a confined space by hydrothermal synthesis.

2.3 Liquid phase coating for confined space

Chemically modifying the inside of a microtube, we can design new chemical interactions within the tube. Creating new chemical interactions, it may be possible to separate target molecules that have been considered difficult to separate. Through our review, we discovered

the importance of the composition in the tube and the chemical interaction with the target molecule.

2.3.1 Liquid phase coating on microtubes

Chemical modification in a confined space is mainly a method using a liquid phase. Using this method, we succeeded in chemically modifying entire confined spaces such as capillaries. Here, we describe the application of chemically modified capillaries fabricated using the sol-gel method.

2.3.2 Mechanism of nanostructured microtubes

Various molecules such as dimethylsiloxane and phenylmethylpolysiloxane have been used to chemically modify the inner walls of microtubes because they can be easily coated by a sol-gel method.[23-28] Their chemistry is used to separate a wide variety of molecules, including high-boiling hydrocarbons and halides.[29-31]Due to this rich variation, there are still a wide variety of capillary tubes for GC-MS and LC-MS.[32-35]However, since most of them are made of organic materials, their heat resistance is low, and repeated experiments may not be reproducible. In addition, since the sol-gel method is a method in which a solution is supplied and the inner wall of the tube is modified by heating or the like, it is difficult to finely control the film thickness, making coating difficult. such as monolithic columns. In the future, if it becomes possible to

chemically modify a structure such as a monolithic column that can be separated with high efficiency so that it can be uniformly coated, we may be able to present further possibilities for experiments using chemical interactions.

2.4 Atomic layer deposition for confined space

Atomic layer deposition (ALD) can provide uniform film thickness control even on very rough acicular nanostructured surfaces.[39-45]However, the applicability of ALD to confined spaces such as tubes has been limited.[46-47]As a result of investigation, we found that gas supply is important for ALD in a confined space.

2.4.1 ALD growth method application examples

Much research has been done on ALD in confined spaces, and experiments have been conducted mainly in two ways. The first is called the flow method and is the standard method.[39-47]This is a method to create a state in which gas flow is always generated in the chamber by constantly supplying gas (N2 gas) into the chamber and exhausting it. By supplying the film-forming raw material (precursor or H2O) contained in the gas flow, film formation is performed in the region reached by the gas. The rest of the supplied raw material gas that is no longer needed for film formation is discharged by the gas flow. This is a method of repeating this

exhaust and supply. The next method is called the exposure method.[48,49] In this method, the gas in the chamber does not always flow, and the gas in the chamber is diffused by stopping the supply of the gas when the precursor is supplied into the chamber and evacuating the gas. Thereby, a film can be formed by supplying a gas to the inside of a sample having pores.

A feature of ALD is that only one atomic layer can be formed in one cycle. The basic principle is that the precursors used are raw materials that react only with hydroxyl groups, so the supplied precursors can only adsorb to the hydroxyl groups in the sample. Precursors that remain unadsorbed are discharged. The surface of the precursor adsorbed on the sample becomes in a state with hydroxyl groups again by the next supply of H2O or ozone. By supplying a new precursor to the hydroxyl group, it becomes possible to form a film at the atomic layer level.

In order to perform ALD in a confined space such as a tube, it is necessary to supply gas inside the tube.[50-58]Because the inner diameter of the tube is small and the conductance decreases as the length increases, little gas is delivered to a given region within the tube, and little gas is delivered to the surrounding chamber. To address this issue, M. Nolan et al. By arranging the tube samples in parallel and filling the chamber with the tubes, we created an environment in which gas was forcibly supplied to the tubes, and succeeded in forming the film.[57] T. Gong et al. In addition to arranging the samples in parallel, by applying a pressure difference between the upstream and downstream sides of the tube, a convection is generated

inside the tube, creating a mechanism for forcibly supplying gas.[56]By controlling the gas supply in this way, ALD can be said to be a device with infinite possibilities.

2.5 Conclusions

Chapter II reviews the literature on structural and chemical modification, including liquid phase coating and ALD. The important implications of this study can be summarized as follows.

- Modification of confined spaces with nanostructures includes preparation of monolithic columns by sol-gel method and hydrothermal synthesis in microchannels. Monolith columns have been successfully used to separate a wide variety of molecules due to their surface area but are not suitable for labile molecules as they require high flow forces to feed the molecules. On the other hand, microchannels are suitable for separating molecules such as DNA because nanostructures can be grown freely, but they are currently grown only in an open environment.
- The sol-gel method is the mainstream for chemical coating on general microtubes. The sol-gel method has been used to coat a wide variety of molecules, starting with the simple method of injecting and drying a liquid phase. However, coating on nanostructures is difficult because it is difficult to control and uniform the film thickness.
- We found that ALD, which can control coatings at the atomic layer level, can only form

films within the range in which the gas can be supplied. In the literature, various ALD devices have been developed to form films on the inner walls of tubes, but we found that there is still an area left unfulfilled.

Solving these problems will create nanostructures of new materials within microtubes, contributing to previously unattainable molecular separations. Therefore, in this paper, we describe a chemical coating method for fabricating novel nanostructures inside microtubes.

2.6 References

[1] Hosoya, Ken, Natsuki Hira, Katsuya Yamamoto, Masaru Nishimura, and Nobuo Tanaka. 2006. "High-Performance Polymer-Based Monolithic Capillary Column." *Analytical Chemistry* 78 (16): 5729–35.

[2] Hong, Tingting, Xi Yang, Yujing Xu, and Yibing Ji. 2016. "Recent Advances in the Preparation and Application of Monolithic Capillary Columns in Separation Science." *Analytica Chimica Acta* 931 (August): 1–24.

[3] Saito, Yoshihiro, Kiyokatsu Jinno, and Tyge Greibrokk. 2004. "Capillary Columns in Liquid Chromatography: Between Conventional Columns and Microchips." *Journal of Separation Science* 27 (17-18): 1379–90.

[4] Koeck, Rainer, Martin Fischnaller, Rania Bakry, Richard Tessadri, and Guenther K. Bonn. 2014. "Preparation and Evaluation of Monolithic poly(N-Vinylcarbazole-Co-1,4-Divinylbenzene) Capillary Columns for the Separation of Small Molecules." *Analytical and Bioanalytical Chemistry* 406 (24): 5897–5907.

[5] Yang, Shengchao, Fanggui Ye, Qinghui Lv, Cong Zhang, Shufen Shen, and Shulin Zhao. 2014. "Incorporation of Metal-Organic Framework HKUST-1 into Porous Polymer Monolithic Capillary Columns to Enhance the Chromatographic Separation of Small Molecules." *Journal of Chromatography. A* 1360 (September): 143–49.

[6] Wu, Minghuo, Ren 'an Wu, Zhenbin Zhang, and Hanfa Zou. 2011. "Preparation and Application of Organic-Silica Hybrid Monolithic Capillary Columns." *Electrophoresis* 32 (1): 105–15.

[7] Chambers, Stuart D., Frantisek Svec, and Jean M. J. Fréchet. 2011. "Incorporation of Carbon Nanotubes in Porous Polymer Monolithic Capillary Columns to Enhance the Chromatographic Separation of Small Molecules." *Journal of Chromatography. A* 1218 (18): 2546–52.

[8] Yusuf, Kareem, Ahmed Yacine Badjah-Hadj-Ahmed, Ahmad Aqel, and Zeid Abdullah ALOthman. 2015. “Fabrication of Zeolitic Imidazolate Framework-8-Methacrylate Monolith Composite Capillary Columns for Fast Gas Chromatographic Separation of Small Molecules.” *Journal of Chromatography. A* 1406 (August): 299–306.

[9] Yasui, Takao, Takeshi Yanagida, Taisuke Shimada, Kohei Otsuka, Masaki Takeuchi, Kazuki Nagashima, Sakon Rahong, et al. 2019. “Engineering Nanowire-Mediated Cell Lysis for Microbial Cell Identification.” *ACS Nano* 13 (2): 2262–73.

[10] Chen, Zhen, Shi-Bo Cheng, Pan Cao, Quan-Fa Qiu, Yan Chen, Min Xie, Yu Xu, and Wei-Hua Huang. 2018. “Detection of Exosomes by ZnO Nanowires Coated Three-Dimensional Scaffold Chip Device.” *Biosensors & Bioelectronics* 122 (December): 211–16.

[11] Yasui, Takao, Takeshi Yanagida, Satoru Ito, Yuki Konakade, Daiki Takeshita, Tsuyoshi Naganawa, Kazuki Nagashima, et al. 2017. “Unveiling Massive Numbers of Cancer-Related Urinary-microRNA Candidates via Nanowires.” *Science Advances* 3 (12): e1701133.

[12] Hisey, Colin L., Kalpana Deepa Priya Dorayappan, David E. Cohn, Karuppaiyah Selvendiran, and Derek J. Hansford. 2018. “Microfluidic Affinity Separation Chip for Selective Capture and Release of Label-Free Ovarian Cancer Exosomes.” *Lab on a Chip* 18 (20): 3144–53.

[13] Maeki, Masatoshi, Yuka Fujishima, Yusuke Sato, Takao Yasui, Noritada Kaji, Akihiko Ishida, Hirofumi Tani, Yoshinobu Baba, Hideyoshi Harashima, and Manabu Tokeshi. 2017. “Understanding the Formation Mechanism of Lipid Nanoparticles in Microfluidic Devices with Chaotic Micromixers.” *PloS One* 12 (11): e0187962.

[14] Suwatthanarak, Thanawat, Ivan Adiyasa Thiodorus, Masayoshi Tanaka, Taisuke Shimada, Daiki Takeshita, Takao Yasui, Yoshinobu Baba, and Mina Okochi. 2021. “Microfluidic-Based Capture and Release of Cancer-Derived Exosomes via Peptide–nanowire Hybrid Interface.” *Lab on a Chip* 21 (3): 597–607.

[15] Yasui, Takao, Noritada Kaji, Ryo Ogawa, Shingi Hashioka, Manabu Tokeshi, Yasuhiro Horiike, and Yoshinobu Baba. 2011. "DNA Separation in Nanowall Array Chips." *Analytical Chemistry* 83 (17): 6635–40.

[16] Yasui, Takao, Sakon Rahong, Koki Motoyama, Takeshi Yanagida, Qiong Wu, Noritada Kaji, Masaki Kanai, et al. 2013. "DNA Manipulation and Separation in Sublithographic-Scale Nanowire Array." *ACS Nano* 7 (4): 3029–35.

[17] Rahong, Sakon, Takao Yasui, Takeshi Yanagida, Kazuki Nagashima, Masaki Kanai, Annop Klamchuen, Gang Meng, et al. 2014. "Ultrafast and Wide Range Analysis of DNA Molecules Using Rigid Network Structure of Solid Nanowires." *Scientific Reports* 4 (June): 5252.

[18] Rahong, Sakon, Takao Yasui, Takeshi Yanagida, Kazuki Nagashima, Masaki Kanai, Gang Meng, Yong He, et al. 2015. "Three-Dimensional Nanowire Structures for Ultra-Fast Separation of DNA, Protein and RNA Molecules." *Scientific Reports* 5 (June): 10584.

[19] Rahong, Sakon, Takao Yasui, Noritada Kaji, and Yoshinobu Baba. 2016. "Recent Developments in Nanowires for Bio-Applications from Molecular to Cellular Levels." *Lab on a Chip* 16 (7): 1126–38.

[20] Yasui, Takao, Takeshi Yanagida, Satoru Ito, Yuki Konakade, Daiki Takeshita, Tsuyoshi Naganawa, Kazuki Nagashima, et al. 2017. "Unveiling Massive Numbers of Cancer-Related Urinary-microRNA Candidates via Nanowires." *Science Advances* 3 (12): e1701133.

[21] Choi, Han-Seok, Mohammad Vaseem, Sang Gon Kim, Yeon-Ho Im, and Yoon-Bong Hahn. 2012. "Growth of High Aspect Ratio ZnO Nanorods by Solution Process: Effect of Polyethyleneimine." *Journal of Solid State Chemistry* 189 (May): 25–31.

[22] Xu, Sheng, and Zhong Lin Wang. 2011. "One-Dimensional ZnO Nanostructures: Solution Growth and Functional Properties." *Nano Research* 4 (11): 1013–98.

[23] Yang, Li, Elizabeth Guihen, and Jeremy D. Glennon. 2005. "Alkylthiol Gold Nanoparticles

in Sol-Gel-Based Open Tubular Capillary Electrochromatography." *Journal of Separation Science* 28 (8): 757–66.

[24] Constantin, Stéphane, and Ruth Freitag. 2000. "Preparation of Stationary Phases for Open-Tubular Capillary Electrochromatography Using the Sol–gel Method." *Journal of Chromatography. A* 887 (1): 253–63.

[25] Wang, Y. C., Z. R. Zeng, C. H. Xie, N. Guan, and E. Q. Fu. 2001. "Use of the Sol-Gel Technique to Prepare Capillary Columns Coated with a Macrocyclic Dioxopolyamine for Open-Tubular Capillary Electrochromatography." *Chromatographia*. https://link.springer.com/article/10.1007/BF02491202.

[26] Liang, Minmin, Meiling Qi, Changbin Zhang, and Ruonong Fu. 2004. "Peralkylated-β-Cyclodextrin Used as Gas Chromatographic Stationary Phase Prepared by Sol–gel Technology for Capillary Column." *Journal of Chromatography. A* 1059 (1): 111–19.

[27] Guo, Yong, and Luis A. Colon. 1995. "A Stationary Phase for Open Tubular Liquid Chromatography and Electrochromatography Using Sol-Gel Technology." *Analytical Chemistry* 67 (15): 2511–16.

[28] Sakai-Kato, Kumiko, Masaru Kato, Haruna Nakakuki, and Toshimasa Toyo'oka. 2003. "Investigation of Structure and Enantioselectivity of BSA-Encapsulated Sol–gel Columns Prepared for Capillary Electrochromatography." *Journal of Pharmaceutical and Biomedical Analysis* 31 (2): 299–309.

[29] Kato, Masaru, Maria T. Dulay, Bryson D. Bennett, Joselito P. Quirino, and Richard N. Zare. 2001. "Photopolymerized Sol–gel Frits for Packed Columns in Capillary Electrochromatography." *Journal of Chromatography. A* 924 (1): 187–95.

[30] Shende, Chetan, Abuzar Kabir, Eric Townsend, and Abdul Malik. 2003. "Sol-Gel Poly(ethylene Glycol) Stationary Phase for High-Resolution Capillary Gas Chromatography." *Analytical Chemistry* 75 (14): 3518–30.

[31] Liu, Xin, Shucheng Sun, Rongbin Nie, Jicheng Ma, Qishu Qu, and Li Yang. 2018. "Highly

Uniform Porous Silica Layer Open-Tubular Capillary Columns Produced via in-Situ Biphasic sol–Gel Processing for Open-Tubular Capillary Electrochromatography." *Journal of Chromatography. A* 1538 (February): 86–93.

[32] Wang, Dongxin, Sau L. Chong, and Abdul Malik. 1997. "Sol−Gel Column Technology for Single-Step Deactivation, Coating, and Stationary-Phase Immobilization in High-Resolution Capillary Gas Chromatography." *Analytical Chemistry* 69 (22): 4566–76.

[33] Kato, Masaru, Nozomi Matsumoto, Kumiko Sakai-Kato, and Toshimasa Toyo'oka. 2003. "Investigation of Chromatographic Performances and Binding Characteristics of BSA-Encapsulated Capillary Column Prepared by the Sol–gel Method." *Journal of Pharmaceutical and Biomedical Analysis* 30 (6): 1845–50.

[34] Hayes, James D., and Abdul Malik. 1997. "Sol–gel Chemistry-Based Ucon-Coated Columns for Capillary Electrophoresis." *Journal of Chromatography. B, Biomedical Sciences and Applications* 695 (1): 3–13.

[35] Hara, Takeshi, Shunta Futagami, Sebastiaan Eeltink, Wim De Malsche, Gino V. Baron, and Gert Desmet. 2016. "Very High Efficiency Porous Silica Layer Open-Tubular Capillary Columns Produced via in-Column Sol–Gel Processing." *Analytical Chemistry* 88 (20): 10158–66.

[36] Pan, Congjie, Weifeng Wang, Huige Zhang, Laifang Xu, and Xingguo Chen. 2015. "In Situ Synthesis of Homochiral Metal–organic Framework in Capillary Column for Capillary Electrochromatography Enantioseparation." *Journal of Chromatography. A* 1388 (April): 207–16.

[37] Gu, Zhi-Yuan, Jun-Qing Jiang, and Xiu-Ping Yan. 2011. "Fabrication of Isoreticular Metal–Organic Framework Coated Capillary Columns for High-Resolution Gas Chromatographic Separation of Persistent Organic Pollutants." *Analytical Chemistry* 83 (13): 5093–5100.

[38] Bigham, Shaun, Jennifer Medlar, Abuzar Kabir, Chetan Shende, Abdel Alli, and Abdul

Malik. 2002. “Sol- Gel Capillary Microextraction.” *Analytical Chemistry* 74 (4): 752–61.

[39] Weber, Matthieu, Boonprakrong Koonkaew, Sebastien Balme, Ivo Utke, Fabien Picaud, Igor Iatsunskyi, Emerson Coy, Philippe Miele, and Mikhael Bechelany. 2017. “Boron Nitride Nanoporous Membranes with High Surface Charge by Atomic Layer Deposition.” *ACS Applied Materials & Interfaces* 9 (19): 16669–78.

[40] Elam, J. W., M. D. Groner, and S. M. George. 2002. “Viscous Flow Reactor with Quartz Crystal Microbalance for Thin Film Growth by Atomic Layer Deposition.” *The Review of Scientific Instruments* 73 (8): 2981–87.

[41] Gao, Feng, Sanna Arpiainen, and Riikka L. Puurunen. 2015. “Microscopic Silicon-Based Lateral High-Aspect-Ratio Structures for Thin Film Conformality Analysis.” *Journal of Vacuum Science & Technology. A, Vacuum, Surfaces, and Films: An Official Journal of the American Vacuum Society* 33 (1): 010601.

[42] Elam, Jeffrey W., Guang Xiong, Catherine Y. Han, H. Hau Wang, James P. Birrell, Ulrich Welp, John N. Hryn, et al. 2006. “Atomic Layer Deposition for the Conformal Coating of Nanoporous Materials.” *Journal of Nanomaterials* 2006 (July). https://doi.org/10.1155/JNM/2006/64501.

[43] Perez, Israel, Erin Robertson, Parag Banerjee, Laurent Henn-Lecordier, Sang Jun Son, Sang Bok Lee, and Gary W. Rubloff. 2008. “TEM-Based Metrology for HfO2 Layers and Nanotubes Formed in Anodic Aluminum Oxide Nanopore Structures.” *Small* 4 (8): 1223–32.

[44] Ladanov, M., P. Algarin-Amaris, G. Matthews, M. Ram, S. Thomas, A. Kumar, and J. Wang. 2013. “Microfluidic Hydrothermal Growth of ZnO Nanowires over High Aspect Ratio Microstructures.” *Nanotechnology* 24 (37): 375301.

[45] Gluch, J., T. Rößler, D. Schmidt, S. B. Menzel, M. Albert, and J. Eckert. 2010. “TEM Characterization of ALD Layers in Deep Trenches Using a Dedicated FIB Lamellae Preparation Method.” *Thin Solid Films* 518 (16): 4553–55.

[46] Becker, Jill S., Seigi Suh, Shenglong Wang, and Roy G. Gordon. 2003. “Highly Conformal Thin Films of Tungsten Nitride Prepared by Atomic Layer Deposition from a Novel Precursor.” *Chemistry of Materials: A Publication of the American Chemical Society* 15 (15): 2969–76.

[47] Cremers, Véronique, Riikka L. Puurunen, and Jolien Dendooven. 2019. “Conformality in Atomic Layer Deposition: Current Status Overview of Analysis and Modelling.” *Applied Physics Reviews* 6 (2): 021302.

[48] Gayle, Andrew J., Zachary J. Berquist, Yuxin Chen, Alexander J. Hill, Jacob Y. Hoffman, Ashley R. Bielinski, Andrej Lenert, and Neil P. Dasgupta. 2021. “Tunable Atomic Layer Deposition into Ultra-High-Aspect-Ratio (>60000:1) Aerogel Monoliths Enabled by Transport Modeling.” *Chemistry of Materials: A Publication of the American Chemical Society* 33 (14): 5572–83.

[49] Elam, J. W., D. Routkevitch, P. P. Mardilovich, and S. M. George. 2003. “Conformal Coating on Ultrahigh-Aspect-Ratio Nanopores of Anodic Alumina by Atomic Layer Deposition.” *Chemistry of Materials: A Publication of the American Chemical Society* 15 (18): 3507–17.

[50] Gordon, R. G., D. Hausmann, E. Kim, and J. Shepard. 2003. “A Kinetic Model for Step Coverage by Atomic Layer Deposition in Narrow Holes or Trenches.” *Chemical Vapor Deposition* 9 (2): 73–78.

[51] Gu, Diefeng, Pragya Shrestha, Helmut Baumgart, Gon Namkoong, and Tarek M. Abdel-Fattah. 2009. “ALD Synthesis of Tube-in-Tube Nanostructures of Transition Metal Oxides by Template Replication.” *ECS Transactions* 25 (4): 191.

[52] Su, C-Y, C-C Wang, Y-C Hsueh, V. Gurylev, C-C Kei, and T-P Perng. 2015. “Enabling High Solubility of ZnO in TiO_2 by Nanolamination of Atomic Layer Deposition.” *Nanoscale* 7 (45): 19222–30.

[53] Mishra, Mrinalini, Chia-Yen Chan, Chi-Chung Kei, Yin-Cheng Yen, Ming-Wei Liao, and

Tsong-Pyng Perng. 2018. “Forced Flow Atomic Layer Deposition of TiO2 on Vertically Aligned Si Wafer and Polysulfone Fiber: Design and Efficacy of Conduit Plates and Soak Function.” *The Review of Scientific Instruments* 89 (10): 105108.

[54] Mishra, Mrinalini, Chi-Chung Kei, Yu-Hsuan Yu, Wei-Szu Liu, and Tsong-Pyng Perng. 2017. “Uniform Coating of Ta2O5 on Vertically Aligned Substrate: A Prelude to Forced Flow Atomic Layer Deposition.” *The Review of Scientific Instruments* 88 (6): 065103.

[55] Chen, Hsueh-Shih, Po-Hsun Chen, Jeng-Liang Kuo, Yang-Chih Hsueh, and Tsong-Pyng Perng. 2014. “TiO2 Hollow Fibers with Internal Interconnected Nanotubes Prepared by Atomic Layer Deposition for Improved Photocatalytic Activity.” *RSC Advances* 4 (76): 40482–86.

[56] Gong, Ting, Longfei Hui, Jianwei Zhang, Daoan Sun, Lijun Qin, Yongmei Du, Chunying Li, Jian Lu, Shenlin Hu, and Hao Feng. 2015. “Atomic Layer Deposition of Alumina Passivation Layers in High-Aspect-Ratio Tubular Reactors for Coke Suppression during Thermal Cracking of Hydrocarbon Fuels.” *Industrial & Engineering Chemistry Research* 54 (15): 3746–53.

[57] Nolan, Mark, Ian Povey, Simon Elliot, Nicolas Cordero, Martyn Pemble, Brian Shortt, and Marcos Bavdaz. 2012. “Uniform Coating of High Aspect Ratio Surfaces through Atomic Layer Deposition.” In *Space Telescopes and Instrumentation 2012: Ultraviolet to Gamma Ray*, 8443:1086–93. SPIE.

Chapter III

Rational Strategy for Space-Confined Seeded Growth of ZnO Nanowires in Meter-Long Microtubes

3.1 Introduction

Designing inner surface chemical properties of confined spaces is an important research subject to create novel chemical events.[1-6] Clearly, the inner surface characteristics dominantly determine the chemical interaction to target molecules within spaces. Among various surface modification methods on inner surfaces of confined spaces, a seeded crystal growth method of inorganic solid nanostructures offers a unique approach. [7-18] This is because inorganic solid surface modifications are thermally robust, which differs from conventional organic molecule surface modifications.[7-18] Furthermore, the seeded crystal growth enables to spatially design the position of nanostructures within confined spaces via positioning the seeds, which are hardly attainable to other surface modification methods.[8,13] However, such seeded crystal growth within confined spaces inherently tends to be difficult as the aspect ratio of confined spaces increases due to confinement effects.[19-20] Since a longer confined space increases the probability of interaction between molecules and inner surfaces, *e.g.* a longer capillary column in general is preferred for liquid phase separations, [21] developing a rational methodology to enable a seeded crystal growth of nanostructures within confined spaces is required.

Here we report a space-confined seeded growth of ZnO nanowires within meter-long microtubes of 100 μm diameter with the aspect ratio up to 10000. ZnO nanowires were grown via seeded hydrothermal crystal growth for relatively short microtubes below the length of 40 mm, while any ZnO nanostructures were not observable at all for longer microtubes.

Microstructural and mass-spectrometric analysis revealed that a conventional seed layer formation using zinc acetate is impossible within the confined space for long microtubes. To overcome this space-confined issue, a flow-assisted seed layer formation is proposed. This flow-assisted method enables us to grow spatially uniform ZnO nanowires even for 1m-long microtubes with the aspect ratio up to 10000. Finally, we investigated a possibility of using the nanowire- microtubes as a separation medium in liquid chromatography (LC). In general, particle packed or monolithic columns are employed in liquids phase separations.[22-25] Open-tubular columns can be utilized only in gas chromatography and micro fluidics[26-27] because the molecular diffusion is not enough in liquid phase separations. The achievement of an effective liquid phase separation with an open-tubular column provides ultra-low-pressure analysis such in LC. Herein, we anticipate that the strong intermolecular interactions based on the ZnO nanowires contribute for the liquid phase separation.

3.2 Seeded crystal growth of hydrothermal ZnO nanostructures within microtubes

Fig.1a illustrates the flow chart of a series of experiments to perform a seeded crystal growth of hydrothermal ZnO nanostructures within microtubes (inner diameter: 100 μm). This experimental procedure consists of two steps, the first step is a formation of ZnO seed layer within a microtube using zinc acetate, and the second step is a formation of ZnO nanowires on

the fabricated seed layers using zinc nitrate. The other detailed experimental conditions employed can be seen in Method section.[28-34] Fig.1b shows the effect of microtube length on scanning electron microscope (SEM) images of inner surfaces at the center position of microtube. The microtube length was varied from 20 to 120 mm. We estimated the nanowire density from the SEM images, as shown in Fig.1c. As clearly seen in the images and estimated data, ZnO nanowires could be grown via seeded hydrothermal crystal growth for relatively short microtubes below the length of 40mm, while any ZnO nanostructures were not observable at all for longer microtubes. The geometrical sizes of fabricated ZnO nanowires are typically 200-300 nm in the diameter and 2-3 μm in the height. Although these data are at the center position of microtube, the spatial uniformity of the presence of nanowires (L = 20, 40 mm) or the absence of nanostructures (L = 60 - 120 mm) was consistently observed for all microtubes. Thus, these experimental results highlight the limitation of conventional seeded hydrothermal crystal growth of ZnO nanowires within long microtubes.

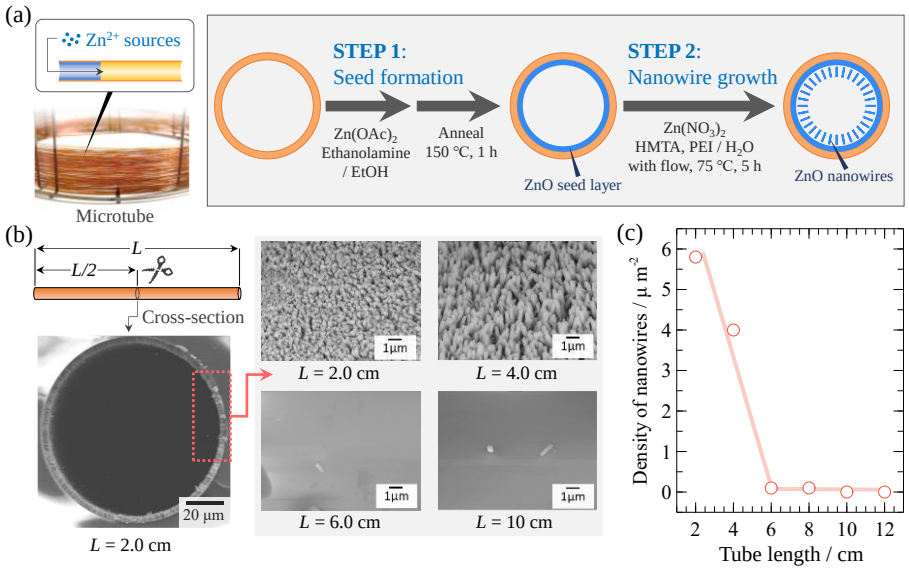

Fig. 1 (a) Schematic of two steps-experimental procedures for a seeded crystal growth of hydrothermal ZnO nanowires within a microtube, (b) SEM images of ZnO nanowire-decorated microtube when varying the length, (c) Relationship between the microtube length and the ZnO nanowire density at the center of microtube.

3.3 Investigation of the cause of poor hydrothermal crystal growth by EDS

Next, we question what causes above observed length limitation of seeded hydrothermal crystal growth of ZnO nanowires for microtubes. The most plausible mechanism is based on the confinement effect within microtubes, which might alter the chemical reaction pathways during seed layer formation and/or nanowire formation. First, we examine such confinement effect on ZnO seed layer formations using zinc acetate (step1 in Fig1a). In order to investigate such effect, we study whether the fabricated ZnO seed layer is soluble in water or not. This is

because such water-soluble substances no longer play a role as seed layers for hydrothermal ZnO nanowires in aqueous solution of reactants in the hydrothermal growth. As illustrated in Fig.2a, we examine such effect by preforming a rinse with water after ZnO seed layer formations. Fig.2b shows energy dispersive x-ray spectroscopy (EDS) data to reveal the presence of zinc compounds after water rinse treatments when varying the length of microtubes (20 mm and 100 mm). Clearly, there is a difference between the two samples on the presence of ZnO seed layers. For the capillary column with the length of 20 mm, the presence of Zn-related compounds was confirmed. On the other hand, any Zn-related compounds were not observable for the microtube with the length of 100 mm. Thus, these results imply that altering a water solubility of zinc related compounds consisting of the seed layer is responsible for the observed experimental trend on the microtube length dependence in Fig.1b-c.

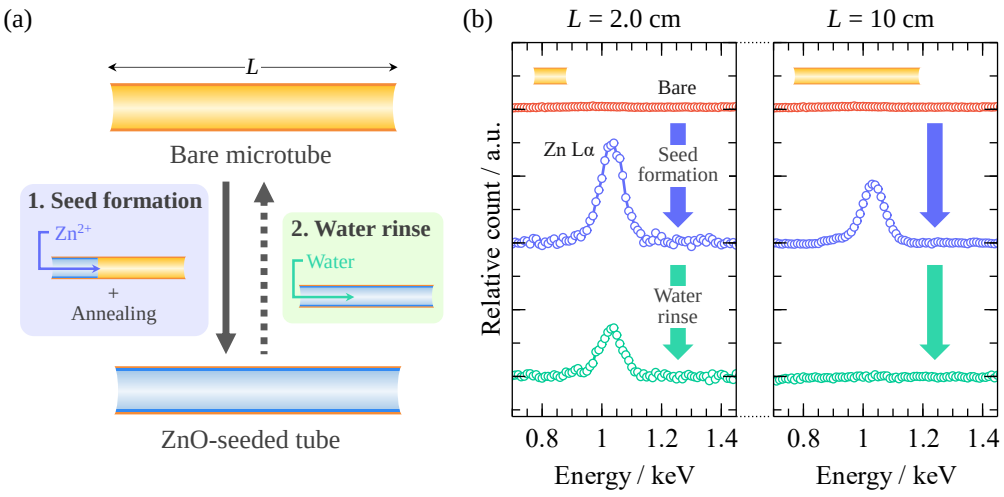

Fig. 2 (a) Schematic of experiments to examine a water solubility of formed ZnO seed layers within a microtube, (b) Effect of microtube length on EDS spectra (Zn Lα) of inner surfaces of ZnO-decorated microtubes when performing a seed layer formation and a water rinse treatments.

3.4 Investigation of the cause of poor hydrothermal crystal growth by GC-MS

Although there is a correlation between nanowire formations in Fig.1 and seed layer formation process in Fig.2, we still have no experimental evidences to explain how a seed layer formation using zinc acetate is altered by increasing a microtube length. Therefore, we analyze volatile components from microtubes with different lengths after seed layer formation process, as illustrated in Fig.3a. Gas chromatography-mass spectrometry (GC-MS) was utilized for the analysis. Fig.3b shows the comparison between microtubes with different lengths (20 mm and 100 mm) on the GC-MS data. As seen in the chromatogram data, a significant peak at 15.2 min was observed (monitored at m/z=60) only for the longer microtube (100 mm), but not for the shorter microtube (20 mm). The mass fragment pattern of the peak reveals that the compound can be assigned to N-(2-hydroxyethyl)acetamide, which must be closely related to the inherent difference between microtubes with different lengths on the seed layer formation process. Based on this observed compound, Fig.3c illustrates a model to explain the plausible different chemical reaction schemes when varying the length of microtubes. First, a condensation of ethanolamine and acetate gives N-(2-hydroxyethyl)acetamide, which coordinates with Zn2+ to yield water-soluble complex. The complex can dehydrate into ZnO and N-(2-hydroxyethyl)acetamide. The reaction is considered to be reversible. If the microtube is short enough, the amide is immediately eliminated from the system as a gas, and ZnO is continuously

generated according to the Le Chatelier's Principle. On the other hand, in the case of the longer microtubes (>60 mm), a poor exchange of outer and inner atmosphere prevents removal of N-(2-hydroxyethyl)acetamide. The remained N-(2-hydroxyethyl)acetamide promotes the backward reaction to soluble Zn2+ complex and prevent ZnO growth. Thus, these mass-spectrometric data revealed that a conventional seed layer formation using zinc acetate is impossible within the confined space for long microtubes due to the detrimental residual N-(2-hydroxyethyl)acetamide and resultant Zn-complex compounds.

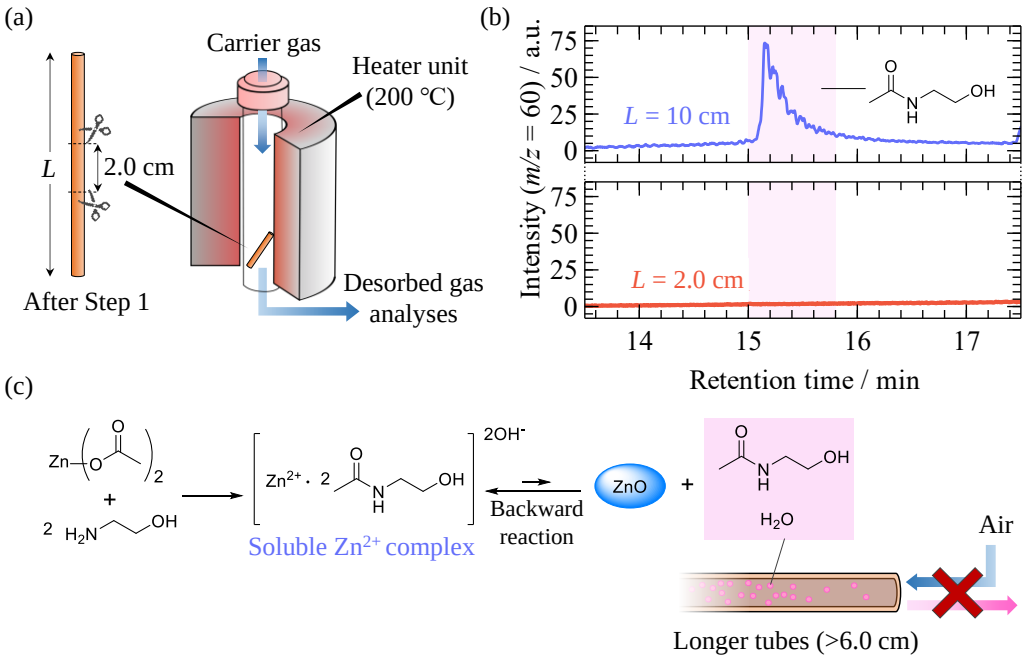

Fig. 3 (a) Schematic of experiments to analyze volatile components from microtubes with different lengths after seed layer formation process, (b) GCMS data of *m/z*=60 for the microtube lengths-20 mm and 100 mm, (c) Possible reaction scheme within a microtube to explain the length dependence on the seed layer formation process.

3.5 ZnO nanowire growth by flow-assisted seed layer formation process

Next, we propose a rational strategy to overcome above limitation of conventional seeded crystal growth of ZnO nanowires for long microtubes. Based on above reaction schemes within confined spaces, it is necessary to remove the detrimental residual products N-(2-hydroxyethyl)acetamide during ZnO seed layer formation process. Thus, we apply air flow process to remove the compounds where a small amount of air is introduced a few times into the microtube during heating process for ZnO seed layer formation, as illustrated in Fig.4a. Fig.4b shows the SEM images of inner surfaces at the center position of column when varying the length of microtubes from 20 to 1000 mm by performing above flow-assisted seed layer formation process. The nanowire density data extracted from the SEM images are shown in Fig.4c. As clearly seen in the images, this newly proposed flow-assisted method enables us to grow spatially uniform ZnO nanowires even for longer microtube (up to 1000 mm) with the aspect ratio up to 10000, as shown in SEM images of Fig.4c. Thus, the newly proposed flow-assisted method enables to overcome the limitation of seeded crystal growth of hydrothermal ZnO nanowires inside highly confined long microtubes with high aspect ratios.

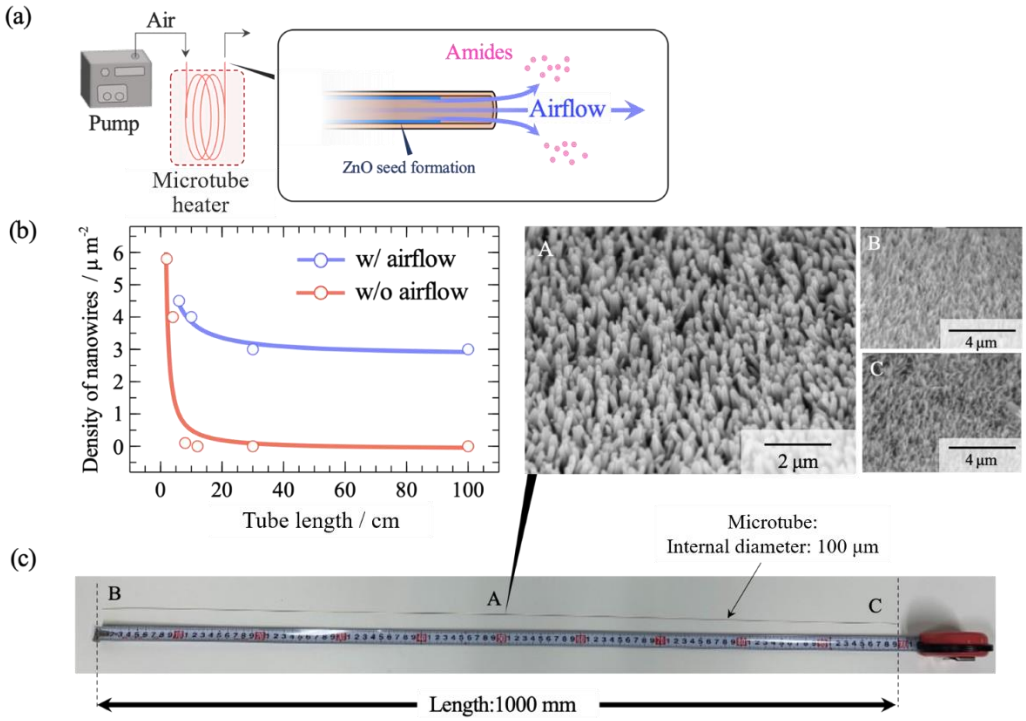

Fig. 4 (a) Schematic of proposed flow-assisted method to enhance a seed layer formation process for longer microtubes, (b) Effect of flow-assisted method on nanowire density data at the center of microtube, which are extracted from SEM images, (c) Optical image of 1-meter microtube, where ZnO nanowires uniformly are grown, and SEM images of inner surface at the marked positions (A, B, C) of 1-meter microtube with the inner diameter of 100μm.

3.6 Liquid phase separation in ZnO nanowire microtubes

Finally, we examine the applicability of fabricated long microtubes with ZnO nanowires uniformly grown on the inner surface for the liquid phase separations, as illustrated in Fig.5a. We prepared microtubes with ZnO nanowires on the inside wall (L =130 and 300 mm), and compared the retention behavior of aromatic compounds with a bare microtube having

functional groups, -SiOH based on the fused silica by nanoflow-liquid chromatography (nano-LC) system respectively (Fig.5a). Significant differences in the retention behavior of each solute on the nanowire array column were confirmed, although not on the bare microtube. This result clearly indicated that the heteroatoms in the solutes reversibly interacted with ZnO nanowires. In particular, the longer microtube (L = 300 mm) retained the solutes much stronger than the shorter one (L = 130 mm), and more clearly differences in retention time of each solute were confirmed. These strong retentions on the longer microtube were achieved due to the increase the chance of interactions with ZnO nanowires in proportion to the microtube length. Furthermore, we compared the retention behavior with a typical silica-based monolithic column (monolith column). Monolithic columns are generally used in LC for a high through put separation due to the three-dimensional skeleton with micrometer-sized through pores.[35-36] We anticipated that the polar interactions should be worked between surface -SiOH and polar functions groups in the solutes. Interestingly, the order of elution was completely different between the monolith column and the ZnO nanowire-decorated microtube (Fig. 5b). To be more precise, the order of elution was acetophenone, benzyl alcohol, and benzyl amine on the nanowire column, while the order of elution was benzyl amine, acetophenone, and benzyl alcohol on the monolith column respectively. This result clearly indicated that these microtubes possess completely different separation mechanisms. Furthermore, it is noted that the ZnO nanowire microtube shows less than one-tenth of the back pressure of the monolith column

under the same flow rate conditions, which is almost the same as the bare microtube (Fig. 5c). Briefly, a high-speed separation in the high flow rate range could be carried out on nanowire microtubes, not on silica monolithic columns. This extremely lower back pressure was due to the lower packing rate of stationary phase in nanowire microtubes than in monolithic columns. The open tubular column with an ultra-thin layered ZnO nanowires effectively contributed in liquid phase separations. Thus, the fabricated ZnO nanowire-decorated microtubes by the flow-assisted method have the potential to provide separation medias with high efficiency and low back pressures for LC.

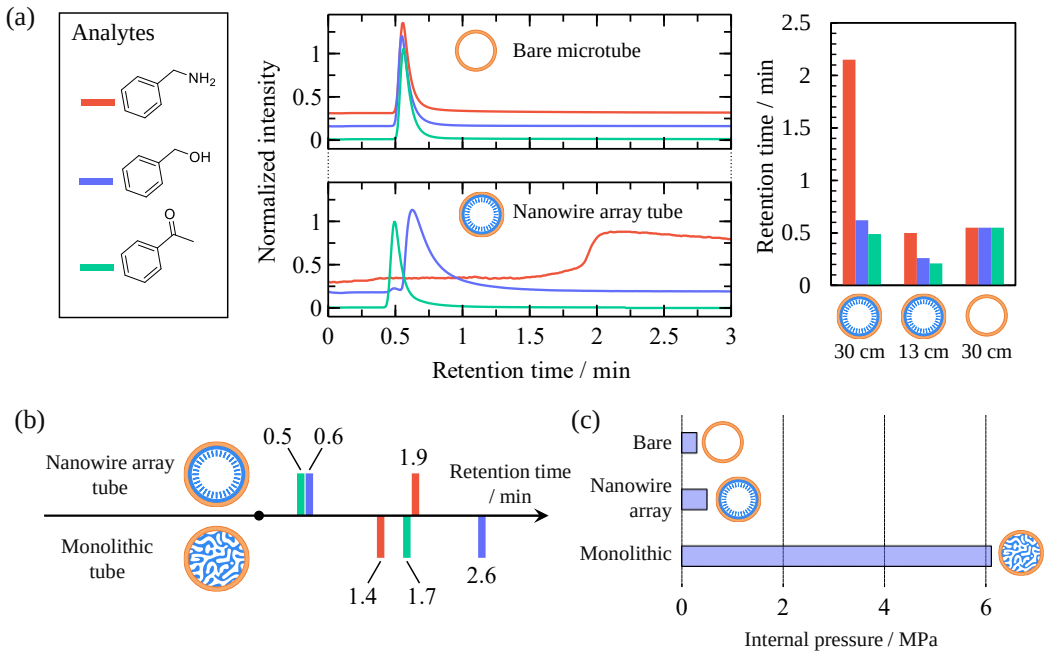

Fig. 5 (a) Chromatograms of sample solutes in each microtube. Green plots show acetophenone, blue plots show benzyl alcohol and red plots show benzyl amine, respectively. Comparison of retention time in each microtube is also shown when varying the microtube length. Conditions: microtube, w/o nanowires (300 mm × 100 μm i.d.), With nanowires (125 mm × 100 μm i.d. and 300 mm × 100 μm

i.d.); flow rate, 5.0 μL min^{-1}; mobile phase, *n*-hexane; detection, UV 254 nm; temperature, 25.0 ^{o}C. (b) Comparison between the ZnO nanowire microtubes and conventional monolithic columns on the retention time, (c) Comparison between ZnO nanowire microtube, bare microtube, monolithic capillary column on the internal pressures required for experiments.

3.7 Reference

[1] Daiguji, H.; Yang P.; Majumdar A. Ion Transport in Nanofluidic Channels. *Nano Lett.* **2004**, 4, 137-142.

[2] Green, Y.; Eshel, R.; Park, S.; Yossifon, G. Interplay between Nanochannel and Microchannel Resistances. Nano Lett. 2016, 16, 2744-2748.

[3] Wang, M.; Cheng, B.; Yang, Y.; Liu, H.; Huang, G.; Han, L.; Li, F.; Xu, F. Microchannel Stiffness and Confinement Jointly Induce the Mesenchymal-Amoeboid Transition of Cancer Cell Migration. Nano Lett. 2019, 19, 5949-5958.

[4] Ostler, D.; Kannam, S.K.; Frascoli, F.; Daivis, P.J.; Todd. B.D. Efficiency of Electropumping in Nanochannels. Nano Lett. 2020, 20, 3396-3402.

[5] Kitao, T.; Nagasaka, Y.; Karasawa, M.; Eguchi, T.; Kimizuka, N.; Ishii, K.; Yamada, T.; Uemura, T. Transcription of Chirality from Metal-Organic Framework to Polythiophene. J. Am. Chem. Soc. 2019, 141, 19565-19569.

[6] Daiguji, H. Ion Transport in Nanofluidic Channels. Chem. Soc. Rev. 2010, 39, 901-911.

[7] Hu W.; Lu Z.; Liu Y.; Chen T.; Zhou X.; Li C.M. A Portable Flow-through Fluorescent Immunoassay Lab-on-a-Chip Device using ZnO Nanorod-Decorated Glass Capillaries. Lab Chip, 2013, 13, 1797-1802.

[8] Yasui T.; Rahong S.; Motoyama K.; Yanagida T.; Wu Q.; Kaji N.; Kanai M.; Doi K.; Nagashima K.; Tokeshi M.; Taniguchi M.; Kawano S.; Kawai T.; Baba Y. DNA Manipulation and Separation in Sublithographic-Scale Nanowire Array. ACS Nano 2013, 7, 3029-3035.

[9] Rahong S.; Yasui T.; Yanagida T.; Nagashima K.; Kanai M.; Klamchuen A.; Meng G.; He Y.; Zhuge F.W.; Kaji N.; Kawai T.; Baba Y. Ultrafast and Wide Range Analysis of DNA Molecules Using Rigid Network Structure of Solid Nanowires. Sci. Rep. 2014, 4, 5252.

[10] Wang G.; Shi G.; Wang H.; Zhang Q.; Li Y. In Situ Functionalization of Stable 3D Nest-

Like Networks in Confined Channels for Microfluidic Enrichment and Detection. Adv. Funct. Mater. 2014, 24, 1017-1026.

[11] Hu, W.; Liu Y.; Chen T.; Liu Y.; Li C.M. Hybrid ZnO Nanorod-Polymer Brush Hierarchically Nanostructured Substrate for Sensitive Antibody Microarrays. Adv. Mater., 2015, 27, 181-185.

[12] Rahong S.; Yasui T.; Yanagida T.; Nagashima K.; Kanai M.; Meng G.; He Y.; Zhuge F.W.; Kaji N.; Kawai T.; Baba Y. Three-dimensional Nanowire Structures for Ultra-Fast Separation of DNA, Protein and RNA Molecules. Sci. Rep. 2015, 5, 10584.

[13] Wang G.; Li K.; Purcell F.; Zhao D.; Zhang W.; He Z.; Tan S.; Tang Z.; Wang H.; Reichmanis E. Three-Dimensional Clustered Nanostructures for Microfluidic Surface-Enhanced Raman Detection. ACS Appl. Mater. Interfaces 2016, 8, 24974-24981.

[14] Yasui T.; Yanagida T.; Ito S.; Konakade Y.; Takeshita D.; Naganawa T.; Nagashima K.; Shimada T.; Kaji N.; Nakamura Y.; Adiyasa Thiodorus I.; He Y.; Rahong S.; Kanai M.; Yukawa H.; Ochiya T.; Kawai T.; Baba Y. Unveiling Massive Numbers of Cancer-related Urinary-Micro RNA Candidates via Nanowires. Sci. Adv. 2017, 3, e1701133.

[15] Wu Z.; Zhao D.; Hou C.; Liu L.; Chen J.; Huang H.; Zhang Q.; Duan Y.; Li Y.; Wang H. Enhanced Immunofluorescence Detection of a Protein Marker using a PAA Modified ZnO Nanorod Array-based Microfluidic Device. Nanoscale, 2018, 10, 17663-17670.

[16] Guo L.; Shi Y.; Liu X.; Han Z.; Zhao Z.; Chen Y.; Xie W.; Li X. Enhanced Fluorescence Detection of Proteins using ZnO Nanowires Integrated Inside Microfluidic Chips. Biosens. Bioelectron. 2018, 99, 368-374.

[17] Luo H.; Leprince-Wang Y.; Jing G. Tunable Growth of ZnO Nanostructures on the Inner Wall of Capillary Tubes. J. Phys. Chem. C 2019, 123, 7408-7415.

[18] Zhao D.; Wu Z.; Yu J.; Wang H.; Li Y.; Duan Y. Highly Sensitive Microfluidic Detection of Carcinoembryonic Antigen via a Synergetic Fluorescence Enhancement Strategy based on the Micro/nanostructure Optimization of ZnO Nanorod Arrays and in situ ZIF-8

Coating. Chem. Eng. J. 2020, 383, 123230.

[19] Mouarrawis V,; Plessius R.; van der Vlugt J.I.; Reek J.N.H. Confinement Effects in Catalysis Using Well-Defined Materials and Cages. Front. Chem. 2018, 6, 623.

[20] Wu S.M.; Yang X.Y.; Janiak C. Confinement Effects in Zeolite-Confined Noble Metals. Angew. Chem. Int. Ed. 2019, 58, 12340-12354.

[21] Lam S.C.; Rodriguez E.S.; Haddada P.R.; Paull B. Recent Advances in Open Tubular Capillary Liquid Chromatography. Analyst, 2019, 144, 3464-3482.

[22] Tranchida, P. Q.; Mondello, L. Current-day Employment of the Micro-Bore Open-Tubular Capillary Column in the Gas Chromatography Field. J. Chromatogr. A 2012, 1261, 23-36.

[23] Lee, J.; Lim, S. H. Development of Open-Tubular-Type Micro Gas Chromatography Column with Bump Structures. Sensors 2019, 19, 3706.

[24] Li, M. W. H.; She, J. Y.; Zhu, H. B.; Li, Z. Q.; Fan, X. D. Microfabricated Porous Layer Open Tubular (PLOT) Column. Lab on a Chip 2019, 19, 3979-3987.

[25] Galietti, M. R.; Peulon-Agasse, V.; Cardinael, P.; Fogwill, M. O.; Besner, S.; Gritti, F. G. Turbulent Supercritical Fluid Chromatography in Open-Tubular Columns for High-Throughput Separations. Anal. Chem. 2020, 92, 7409-7412.

[26] Jandera, P.; Hajek, T.; Stankova, M. Monolithic and Core–Shell Columns in Comprehensive Two-Dimensional HPLC: a Review. Anal. Bioanal. Chem. 2015, 407, 139-151.

[27] Ma, S. J.; Li, Y.; Ma, C.; Wang, Y.; Ou, J. J.; Ye, M. L. Challenges and Advances in the Fabrication of Monolithic Bio-separation Materials and their Applications in Proteomics Research. Adv. Mater. 2019, 31, 1902023.

[28] He Y.; Yanagida T.; Nagashima K.; Zhuge F.W.; Meng G.; Xu B.; Klamchuen A.; Rahong S.; Kanai M.; Li X.; Suzuki M.; Kai S.; Kawai T. Crystal-Plane Dependence of Critical Concentration for Nucleation on Hydrothermal ZnO Nanowires. J. Phys. Chem. C 2013, 117, 1197-1203.

[29] Nakamura K.; Takahashi T.; Kanai M.; Zhang G.; Hosomi T.; Seki T.; Nagashima K.; Shibata N.; Yanagida T. Redox-Inactive CO2 Determines Atmospheric Stability of Electrical Properties of ZnO Nanowire Devices through Room-Temperature Surface Reaction. ACS Appl. Mater. Interfaces 2019, 11, 40260-40266.

[30] Sakai D.; Nagashima K.; Yoshida H.; Kanai M.; He Y.; Zhang G.; Zhao X.; Takahashi T.; Yasui T.; Hosomi T.; Uchida Y.; Takeda S.; Baba Y.; Yanagida T. Substantial Narrowing on the Width of "Concentration Window" of Hydrothermal ZnO Nanowires via Ammonia Addition. Sci. Rep. 2019, 9, 14160.

[31] Wang C.; Hosomi T.; Nagashima K.; Takahashi T.; Zhang G.; Kanai M.; Hao Z.; Mizukami W.; Shioya N.; Shimoaka T.; Tamaoka T.; Yoshida H.; Takeda S.; Yasui T.; Baba Y.; Aoki Y.; Terao J.; Hasegawa T.; Yanagida T. Rational Method to Monitor Molecular Transformations on Metal Oxide Nanowire Surfaces. Nano Lett. 2019, 19, 2443-2449.

[32] Wang C.; Hosomi T.; Nagashima K.; Takahashi T.; Zhang G.; Kanai M.; Yoshida H.; Yanagida T. Phosphonic Acid Modified ZnO Nanowire Sensors: Directing Reaction Pathway of Volatile Carbonyl Compounds. ACS Appl. Mater. Interfaces 2020, 12, 44265-44272.

[33] Zhao X.; Nagashima K.; Zhang G.; Hosomi T.; Yoshida H.; Akihiro Y.; Kanai M.; Mizukami W.; Zhu Z.; Takahashi T.; Suzuki M.; Samransuksamer B.; Meng G.; Yasui T.; Aoki Y.; Baba Y.; Yanagida T. Synthesis of Monodispersedly Sized ZnO Nanowires from Randomly Sized Seeds. Nano Lett. 2020, 20, 599-605.

[34] Liu J.; Nagashima K.; Yamashita H.; Mizukami W.; Hosomi T.; Kanai M.; Zhao X.; Miura Y.; Zhang G.; Takahashi T.; Suzuki M.; Sakai D.; He Y.; Yasui T.; Aoki Y.; Baba Y.; Ho J.C.; Yanagida T. Face-Selective Tungstate Ions Drive Zinc Oxide Nanowire Growth Direction and Dopant Incorporation. Commu. Mater., 2020, 1, 58.

[35] Motokawa M.; Kobayashi H.; Ishizuka N.; Minakuchi H.; Nakanishi K.; Jinnai H.; Hosoya K.; Ikegami T.; Tanaka N. Monolithic Silica Columns with Various Skeleton Sizes and

Through-Pore Sizes for Capillary Liquid Chromatography. J Chromatogr A. 2002, 961, 53-63.

[36] Tanaka N.; Kobayashi H.; Nakanishi K.; Minakuchi H.; Ishizuka N. Peer Reviewed: Monolithic LC Columns. Anal. Chem. 2001, 73, 420-429.

[37] Greene L.E.; Law M.; Tan D.H.; Montano M.; Goldberger J.; Somorjai G.; Yang P. General Route to Vertical ZnO Nanowire Arrays Using Textured ZnO Seeds. Nano Lett. 2005, 7, 1231-1236.

[38] Kubo T.; Murakami Y.; Tsuzuki M.; Kobayashi H.; Naito T.; Sano T.; Yan M.; Otsuka K. Unique Separation Behavior of a C60 Fullerene-Bonded Silica Monolith Prepared by an Effective Thermal Coupling Agent. Chem. Eur. J. 2015, 21, 18095-18098.

[39] Kanao, E.; Kubo, T.; Naito, T.; Sano, T.; Yan, M.; Tanaka, N.; Otsuka, K. Tunable Liquid Chromatographic Separation of H/D Isotopologues Enabled by Aromatic π Interactions. Anal. Chem. 2020, 92, 4065-4072.

[40] Kanao, E.; Morinaga, T.; Kubo, T.; Naito, T.; Matsumoto, T.; Sano, T.; Maki, H.; Yan, M.; Otsuka, K. Separation of Halogenated Benzenes Enabled by Investigation of Halogen–π Interactions with Carbon Materials. Chem. Sci. 2020, 11, 409-418.

Chapter IV

Moderate molecular recognitions on ZnO m-planeand their selective capture/release of bio-relatedphosphoric acids

4.1 Introduction

Metal oxides exhibit thermal and chemical stabilities in harsh environments and diverse functional properties such as ferroelectricity, ferromagnetism, high temperature superconductivity, metal-insulator transitions, and memristors.[1–7] Consequently, they have been studied for numerous applications. Since the development of the self-assembly process in the last half of the 20th century, the morphologies of various dimensional nanostructures (e.g., nanoparticles,[8,9] nanosheets,[10,11] nanorods,[12,13] and other characteristic three-dimensional structures[14] consisting of metal oxides) have been elucidated. Nanostructures have a large surface, uniform size, perfect crystals, and anisotropy. They have potential to provide programable and integrated properties in various technological elds, especially in molecular recognition and sensing materials.[15–17]

Wire-like one-dimensional nanostructures (nanowires; NWs) are fascinating nanostructures consisting of metal oxides. NWs have been applied to design gas sensors,[18–20] biosensors,[21,22] optoelectronic devices,[23] and photocatalysts.[24,25] In particular, ZnO NWs are of great interest from industrial perspectives in the materials eld due to their simple syntheses, biocompatibility, biodegradability, and biosafety.[26–30] For example, a ZnO NW semiconductor-based electrical sensor was fabricated to detect nonanal, a biomarker for lung cancer.[31] In addition, biomolecular analysis systems based on specific interactions with biomolecules have been constructed using ZnO NWs. Examples include a highly sensitive and selective ZnO NW

sensor for immunoglobulin G [32] and a ZnO NW microuidic device to detect cancer-related miRNA biomarkers from urinary extracellular vesicles.[33]

Despite the large number of applications, few reports have comprehensively investigated the fundamental mechanism of molecular recognition on ZnO NWs. A detailed understanding of molecular recognition on ZnO NWs should provide information on the rational design of a highly functional device. Liquid chromatography (LC), which is a fundamental and highly versatile separation technique, is suitable to investigate the intermolecular interactions on nanomaterials. LC directly reflects the strength of intermolecular interactions with the given stationary and mobile phases. Previously, we developed novel separation media utilizing nanocarbon materials as the stationary phase and investigated their unique molecular recognitions. These included the spherical recognition of C_{60}- or C_{70}-fullerenes,[34,35] the difference in the intensities of the CH or CD–π interaction,[36,37] the strong CH–π interaction between corannulene and planar polycyclic aromatic hydrocarbons,[38] and specific halogen–π interaction of C_{70}-fullerene.[39] Furthermore, we have grown spatially uniform ZnO NWs in meter-long microtubes with an aspect ratio up to 10 000 (ZnO-NW column) by a new self-assembly strategy called the “flow-assisted method”. [40] This microtube can be used as a separation medium for LC. We confirmed the specific retention of the polar functional groups due to the Lewis acidity of their Zn sites. Consequently, the evaluation of the retention behaviors on the ZnO-NW column may shed light on the molecular recognition of ZnO NWs

in a particular liquid mobile phase.

In this study, we investigate the retention behaviors of various analytes on the ZnO-NW column in LC for a precise understanding of the molecular recognition on ZnO NWs in aqueous solvents. We also demonstrate the potential of nucleotide analysis using ZnO NWs due to the efficient molecular recognition on the $(10\bar{1}0)$ m-planes. Finally, we show effective gradient separation of the nucleotides, which require selective sensing to reveal their roles as energy currencies of cells in cellular activities derived from biological processes such as cell motility, intercellular transport, synthesis of biomolecules, and metabolic reactions.[41–44] We successfully separated adenosine mono-, di-, and triphosphates (AMP, ADP, and ATP) based on specific intermolecular interactions on ZnO NWs by optimizing the aqueous mobile phase and the column length.

4.2 Retention behaviors of monosubstituted benzenes on the ZnO-NW column

To evaluate the fundamental characteristics of the intermolecular interactions on ZnO NWs, we investigated the retention behavior of monosubstituted benzenes with various functional groups in LC on the ZnO-NW column. For comparison, we also examined the retention behavior on a bare capillary column using acetonitrile as the mobile phase. Acetonitrile is commonly used in LC. Fig. 1a–c show the typical chromatograms of benzyl amine, ethyl benzoate, and benzoic acid by the column type, respectively. Benzyl amine and ethyl benzoate

passed through these columns. In contrast, benzoic acid was strongly retained on the ZnO-NW column and was not eluted even after an hour.

We then determined the functional groups with a strong intermolecular interaction on ZnO NWs. The recovery ratio of each analyte on the ZnO-NW column was calculated by comparing the peak areas on the ZnO-NW column to those on the bare capillary column (Fig. 1d). The recovery ratios were calculated as

Recovery ratio = (peak area on the ZnO-NW column)/(peak area on the bare capillary column)

The recovery ratios of benzoic acid, phenylsulfonic acid, and phenylphosphonic acid were drastically reduced on the ZnO NW column. ZnO NWs showed a strong and irreversible intermolecular interaction with acidic functional groups in acetonitrile.

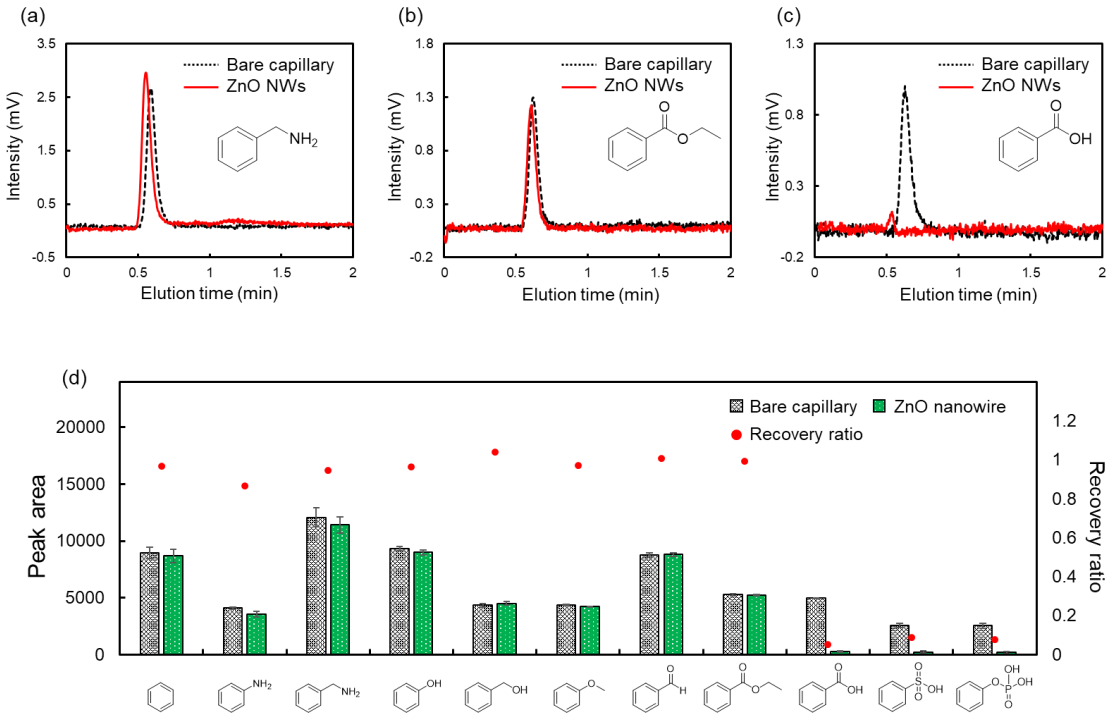

Figure 1. Retention behaviors of monosubstituted benzenes with various functional groups on the ZnO NWs column. Typical chromatograms of (a) benzyl amine, (b) ethyl benzoate and (c) benzoic acid on the ZnO NWs column and the bare capillary column. (d) Peak area and recovery ratio of each compound. LC conditions: Column, ZnO NWs column (30 cm × 100 μm), bare capillary column (30 cm × 100 μm); Mobile phase, acetonitrile; flow rate, 5.0 μL/min; temperature, 25 °C; detection, UV (254 nm).

The specific adsorption of acidic functional groups on ZnO NWs may depend on several factors such as hydrophilic interactions[45,46] and ionic electrostatic interactions.[47–49] We hypothesized that adding water to the mobile phase increases the recovery ratios of these

compounds because water competitively coordinates to ZnO NWs and has a high dielectric constant.[50,51] Fig. 2a shows the recovery ratios of monosubstituted benzenes with acidic functional groups in the mobile phase containing water. As expected, the recovery ratio of each analyte exceeded 80% by adding 20% water to the mobile phase, suggesting that water competitively interacts with ZnO NWs and suppresses the adsorption of monosubstituted benzenes with acidic functional groups. Interestingly, phenylphosphoric acid showed much longer retention times and broader peaks on the ZnO-NW column than the other analytes even in mobile phases containing water (Fig. 2b and c), although the retention time slightly decreased as the content of water in the mobile phase increased. Thus, ZnO NWs interact more strongly with the phosphate groups of the analytes than the other functional groups. The number of negative charges may account for this trend. Zn^{2+}, which is the divalent cation in ZnO NWs, preferred the divalent anion $–PO_3^{2-}$ in phenylphosphoric acid than the other monovalent anions.

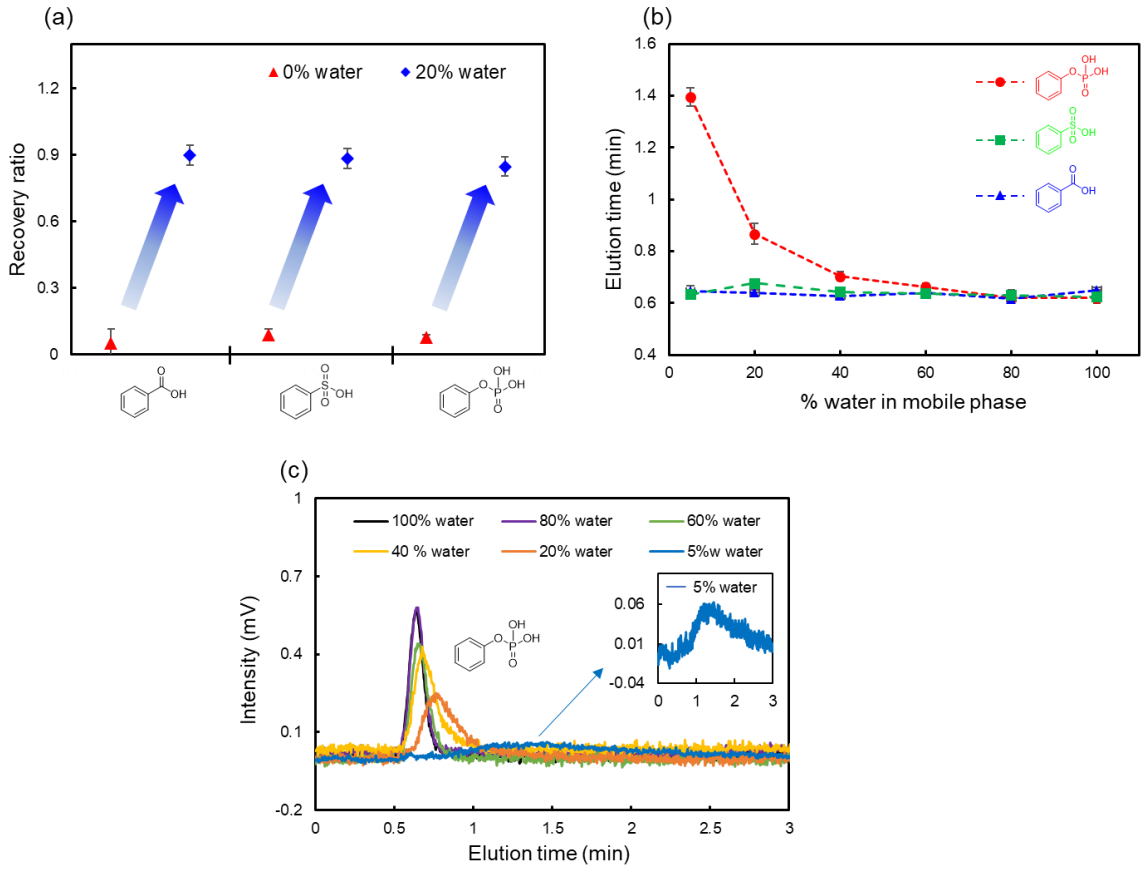

Figure 2. Effect of water content in the mobile phase on retention behaviors of monosubstituted benzenes with acidic functional groups on ZnO NWs. (a) Recovery ratio of each monosubstituted benzene with acidic functional group in acetonitrile containing 20%water as the mobile phase. (b) Plots of retention times of monosubstituted benzenes vs percent water in acetonitrile as the mobile phase. (c) The typical chromatograms of phenyl phosphoric acid in water content mobile phase. LC conditions: Column, ZnO NWs column (30 cm × 100 μm), Bare capillary column (30 cm × 100 μm); Mobile phase, water/acetonitrile; flow rate, 5.0 μL/min; temperature, 25 °C; detection, UV (254 nm).

4.3 Retention behaviors of phosphorylated nucleotides on the ZnO-NW column

ZnO NWs may interact specifically with the phosphate groups in the mobile phase containing water due to hydrophilic and ionic electrostatic interactions. We evaluated the retention behaviors of nucleotides on the ZnO-NW column to test this hypothesis and to explore the potential of applying ZnO NWs to phosphorylated biomolecular analysis. Nucleotides contribute to many biological processes by regulating the concentration and are important for maintaining the cell health and expression of cellular functions.[52–54] Furthermore, they are useful biomarkers for several cancers.[55] Consequently, there is a growing demand for detection or measurement techniques to determine these concentration ratios.

Firstly, we evaluated the retention behaviors of AMP, ADP, and ATP, which are nucleotides found in RNA, on the ZnO-NW column in acetonitrile as the mobile phase. The mobile phase contained 5% water, considering the solubility of nucleotides. For comparison, adenosine, which has the same structure except for the phosphate group, was also evaluated. Fig. 3 shows the retention behaviors of adenosine, AMP, ADP, and ATP in acetonitrile on ZnO-NWs and bare capillary columns. The retention behavior of adenosine was similar for both the ZnO-NW column and the bare capillary column (Fig. 3a and e). On the other hand, the nucleotides were adsorbed on the ZnO-NW column and exhibited drastically reduced recovery ratios (Fig. 3b–

e). These results are consistent with our hypothesis that ZnO NWs show highly selective retention for the phosphate groups. Notably, phosphorylated nucleotides were completely adsorbed on the ZnO-NW column even in the mobile phase containing 5% water but phenylphosphoric acid was eluted (Fig. 2b and c). This stronger interaction of the nucleotides with ZnO NWs than phenylphosphoric acid may be due to the higher hydrophilicity of nucleotides compared to phenylphosphoric acid.

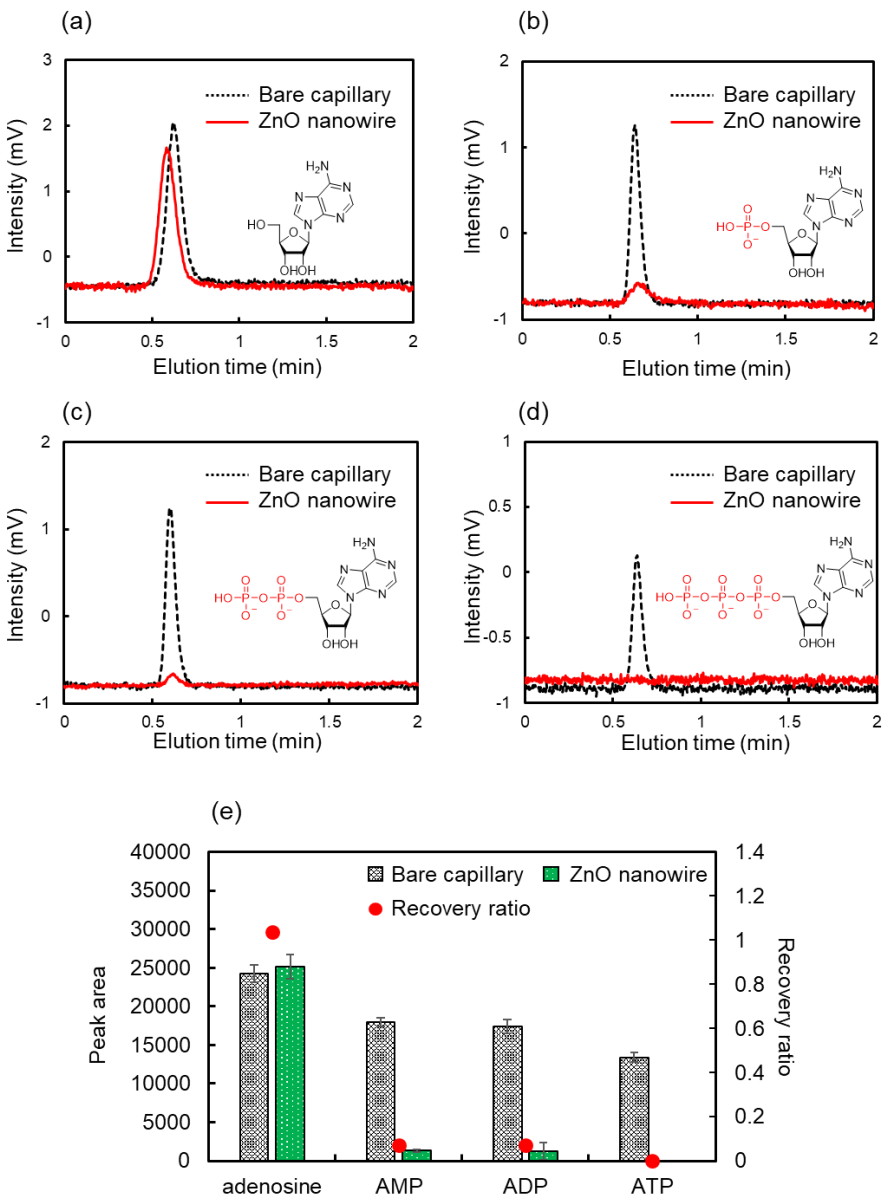

Figure 3. Retention behaviors of adenosine and nucleotides on ZnO NWs column in acetonitrile as the mobile phases. Typical chromatograms of (a) adenosine, (b) AMP, (c) ADP and (d) ATP on ZnO NWs column and the bare capillary column. (e) Peak area and recovery ratio of each compound. LC conditions: Column, ZnO NWs column (30 cm × 100 μm), bare capillary column (30 cm × 100 μm); Mobile phase, acetonitrile containing 5% water; flow rate, 5.0 μL/min; temperature, 25 °C; detection, UV (260 nm).

The suppression of the hydrophilic interactions by molecular recognition in aqueous environments is critical for biomolecular analysis.[56] We evaluated the retention behaviors of nucleotides in pure water as the mobile phase on the ZnO-NW column (Fig. 4). AMP showed a higher recovery ratio in pure water than in acetonitrile but its retention time was longer than adenosine (Fig. 4a, b, and e). This weakened intermolecular interaction between AMP and ZnO NWs may be due to the competitive hydrophilic interaction with water. Interestingly, ADP and ATP adsorbed on the ZnO-NW column, and their recovery ratios were very low even in water (Fig. 4c–e). The recovery ratios on the ZnO-NW column decreased in the order AMP < ADP < ATP, which coincides with the increase in the number of phosphate groups in the nucleotides. Thus, the strength of the intermolecular interactions between ZnO and nucleotides depends on the number of phosphate groups in the nucleotide.

We then examined whether the ZnO NW nanostructure or the typical properties of ZnO lead to the discrimination of the phosphate groups in the nucleotides. We evaluated the recovery ratios of adenosine and nucleotides on a column fabricated only by the ZnO seed layer, which lacks uniform nanostructures but has the same properties as that of ZnO. Both ADP and ATP were fully eluted on the column fabricated using only the ZnO seed layer (Fig. S1†). The discrimination for the phosphate groups of nucleotides on ZnO NWs in water is attributed to

the nanostructures.

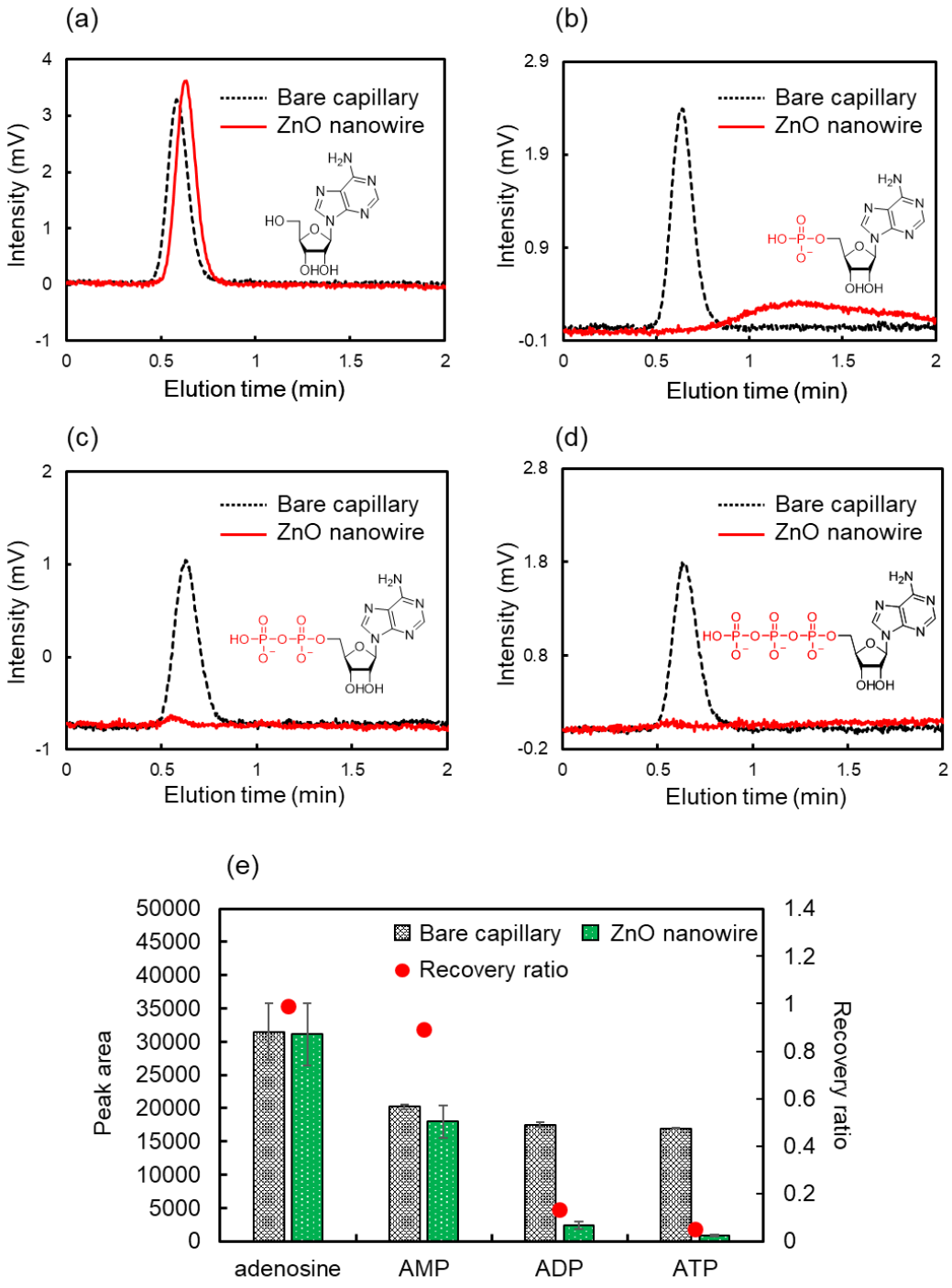

Figure 4. Retention behaviors of adenosine, AMP, ADP and ATP on ZnO NWs column in water as the mobile phases. Typical chromatograms of (a) adenosine, (b) AMP, (c) ADP and (d) ATP on the ZnO NWs column and the bare capillary column. (e) Peak area and recovery ratio of

each analyte. LC conditions: Column, ZnO NWs column (30 cm × 100 μm), Bare capillary column (30 cm × 100 μm); Mobile phase, water; flow rate, 5.0 μL/min; temperature, 25 °C; detection, UV (260 nm).

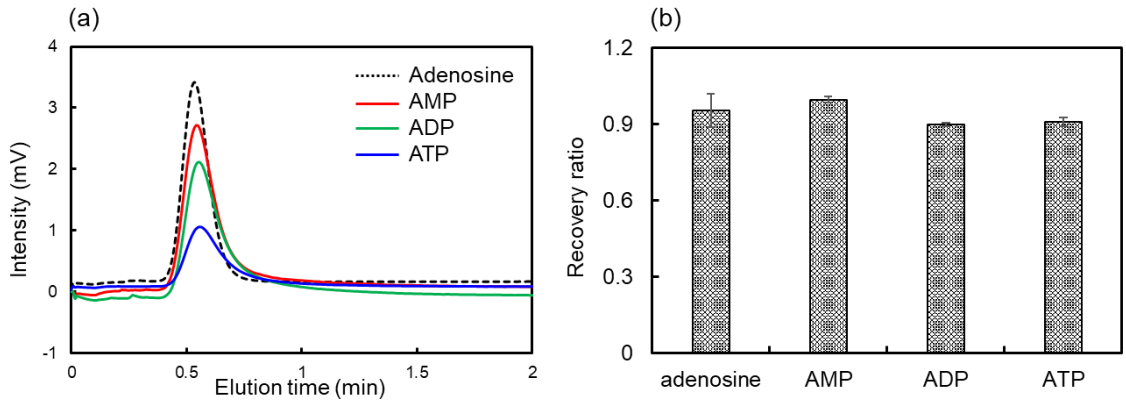

Figure S1. Retention behaviors of adenosine, AMP, ADP and ATP on on the column fabricated only the ZnO seed layer (Seed layer column). (a) Typical chromatograms of adenosine and nucleotides. (b) Recovery ratio of each compound. LC conditions: Column, Seed layer column (30 cm × 100 μm), bare capillary column (30 cm × 100 μm); Mobile phase, water; flow rate, 5.0 μL/min; temperature, 25 °C; detection, UV (260 nm).

4.4 IR spectra of adsorbed nucleotides on the ZnO NWs

Two fundamental aspects should be considered for molecular recognition since the nanostructure is responsible for the phosphate group discrimination of nucleotides on ZnO

NWs: the specific surface area and the morphology. Two types of ZnO nanostructures (ZnO nanowalls and ZnO NWs, Fig. S2†) were fabricated on silicon wafers. IR spectroscopy was used for the molecular recognition of the nucleotide on each nanostructure. The substrate with each nanostructure was immersed into an aqueous solution of AMP, ADP, or ATP (7 mM) and was dried to adsorb the nucleotide on the nanostructure. The substrates were subsequently immersed in water. Then, IR spectroscopy was performed after drying the substrates well.

Fig. 5 shows the IR spectra of the nucleotides on each substrate for different immersion times. Each substrate displayed a narrow band in the range of 900–1200 cm^{-1} , [57,58] which is derived from the phosphate groups, immediately after immersing the substrates into the nucleotide solution (0 min, Fig. 5, black lines). The signal was not confirmed without immersing ZnO NWs in the nucleotides (Fig. S3,† black line) and the intensity was increased with the immersion time (Fig. S3†). These results suggested that the nucleotide was adsorbed on ZnO nanostructures. On the ZnO nanowalls, the band intensity of the phosphate group in the nucleotide was independent of the immersion time in water, indicating that all the nucleotides are completely adsorbed on the ZnO nanowalls, regardless of the number of

phosphate groups (Fig. 5a–c). On the other hand, on the ZnO NWs, the band intensity of the phosphate group in the nucleotides decreased as the immersion time in water increased. More interestingly, although the band intensity in ATP slightly decreased, the decreases in the band intensity were smaller in the order AMP > ADP > ATP (Fig. 5d–f). Briefly, the intermolecular interaction with nucleotides on ZnO NWs was weaker than that on the ZnO nanowalls, whereas the strength varied slightly with the number of phosphate groups in the nucleotides. These results suggest that the discrimination based on the number of phosphate groups in the nucleotides is due to the morphology of ZnO NWs.

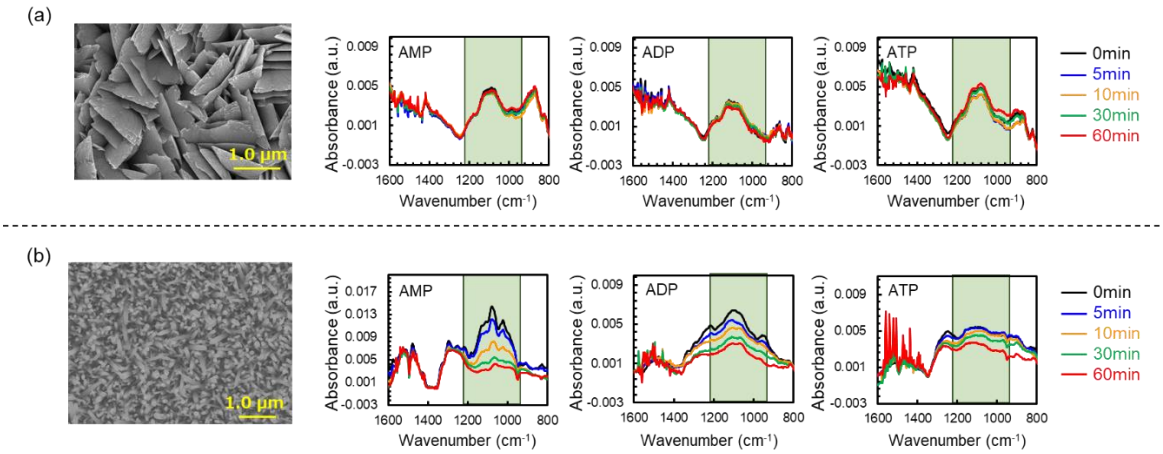

Figure 5. IR peak shifts of phosphorylated nucleotides on ZnO nanostructures with immersion time in water. (a) SEM images of ZnO nanowalls on the silicon wafer and IR spectral comparisons of AMP, ADP and ATP on ZnO nanowalls. (b) SEM images of ZnO NWs on the silicon wafer and IR spectral comparisons of AMP, ADP and ATP on ZnO NWs.

The morphology of the ZnO nanostructures could be controlled by competitive nucleation from the (0001) *c*-planes and *m*-planes. Thus, ZnO NWs and nanowalls provide unique face-selective electrostatic interactions by anisotropic crystal growth.[26,59–63] Fig. S4† shows the SEM image of the top surface of the ZnO NWs. The small hexagonal shape on the top surface and the long columnar shape (Fig. S2†) implied abundant *m*-planes. The ZnO nanowalls and ZnO NWs exposed the *c*-planes and the *m*-planes, respectively. The polar *c*-plane provides a higher ionicity due to the biased surface to either Zn^{2+} or O^{2-}. In contrast, Zn^{2+} and O^{2-} are present in the same proportion on the nonpolar m-plane.[64–66] Therefore, the ZnO nanowalls may indiscriminately adsorb the nucleotides on the *c*-planes via their strong hydrophilic and ionic electrostatic interactions with phosphate groups. On the other hand, ZnO NWs may flexibly recognize the phosphate groups due to their moderate hydrophilic and ionic electrostatic interactions on the *m*-planes.

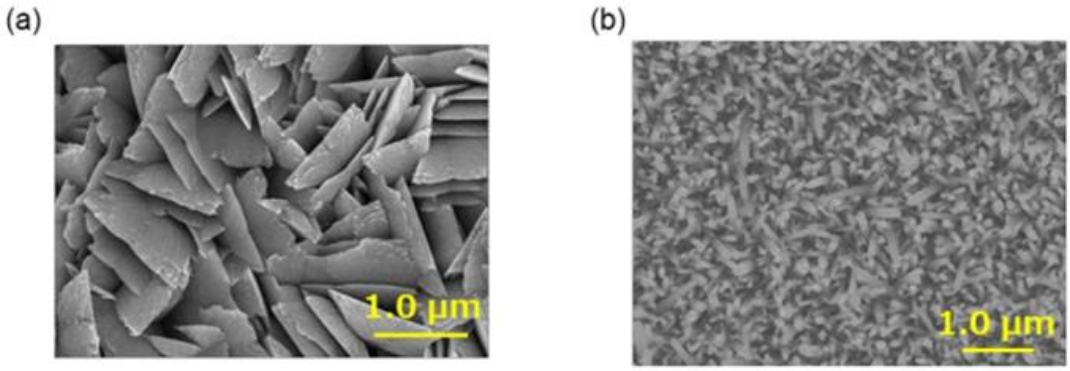

Figure S2. SEM images of (a) ZnO nanowalls and (b) ZnO NWs on silicon wafers.

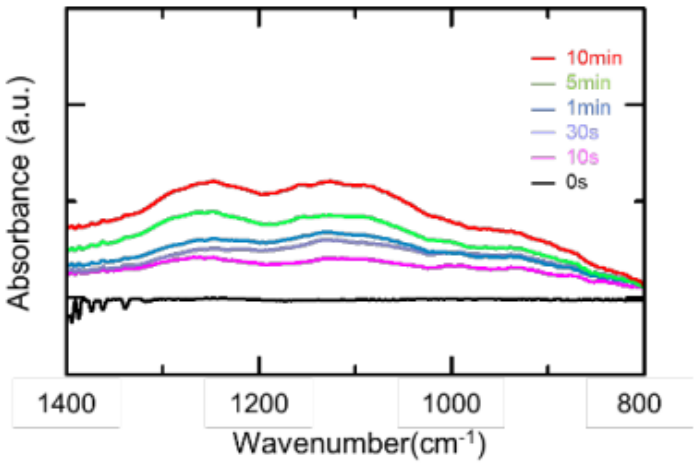

Figure S3. IR peak shifts of ATP on ZnO NWs with different immersion time in ATP solution. The black line shows the IR spectra of ZnO NWs before immersion.

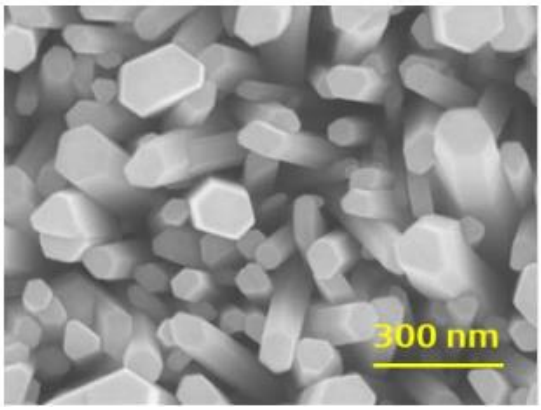

Figure S4. SEM image on the top surface of ZnO NWs.

4.5 Dependence of molecular recognition on the ZnO-NW column on the temperature and flow rate

Ionic electrostatic and hydrophilic interactions may be responsible for the interactions between ZnO NWs and the phosphate groups. The ionic electrostatic interaction is dominant,

especially in water, because the hydrophilic interactions are suppressed. The potential energy of the ionic electrostatic interaction is given as

$$E = z^{+}z^{-}e^{2} / 4\pi\varepsilon R \qquad (1)$$

Here, z^{+} and z^{-} are the valences of the cation and anion, respectively, e is the elementary charge, ε is the dielectric constant, and R is the distance between the cation and the anion.[67] Eqn (1) indicates that the ionic electrostatic interaction is not influenced by the temperature. Furthermore, ionic electrostatic interactions rapidly form even in water.[68] Here, we hypothesized that the interactions of nucleotides on ZnO NWs are not influenced by the temperature or flow rate in LC analysis. Then, we derived the temperature and flow rate dependencies from the plot of the recovery ratios of nucleotides at different temperatures and flow rates (Fig. S5†). The recovery ratios of each nucleotide were almost the same at different temperatures and flow rates, supporting our hypothesis that molecular recognition for nucleotides on ZnO NWs is due to the ionic electrostatic interaction and is independent of the temperature and flow rate. In addition, the SEM images indicate that the measurement does not corrupt ZnO NWs in the capillary column (Fig. S6†). This physical robustness of ZnO NWs may realize stable molecular recognition in harsh physical conditions.

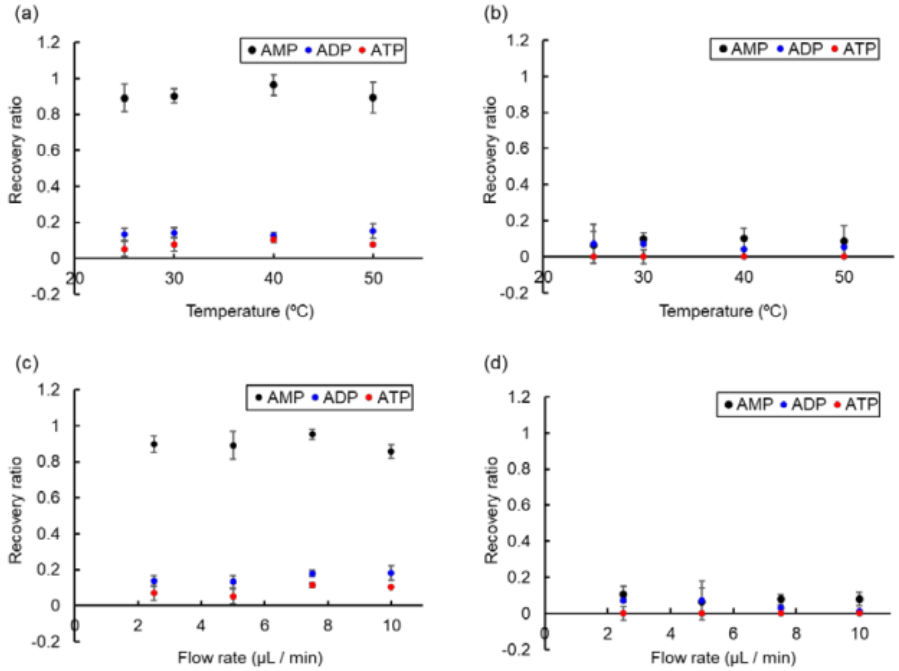

Figure S5. Retention behaviors of nucleotides at different temperatures or flow rates on ZnO NWs column. (a), (b) Plot of recovery ratio of nucleotides vs temperature. (c), (d) Plot of recovery ratio of nucleotides vs flow rate. LC condition: column, ZnO-NWs (30 cm × 100 μm), bare capillary (30 cm × 100 μm); mobile phase, (a), (c) water, (c), (d) ACN; detection, UV (260 nm).

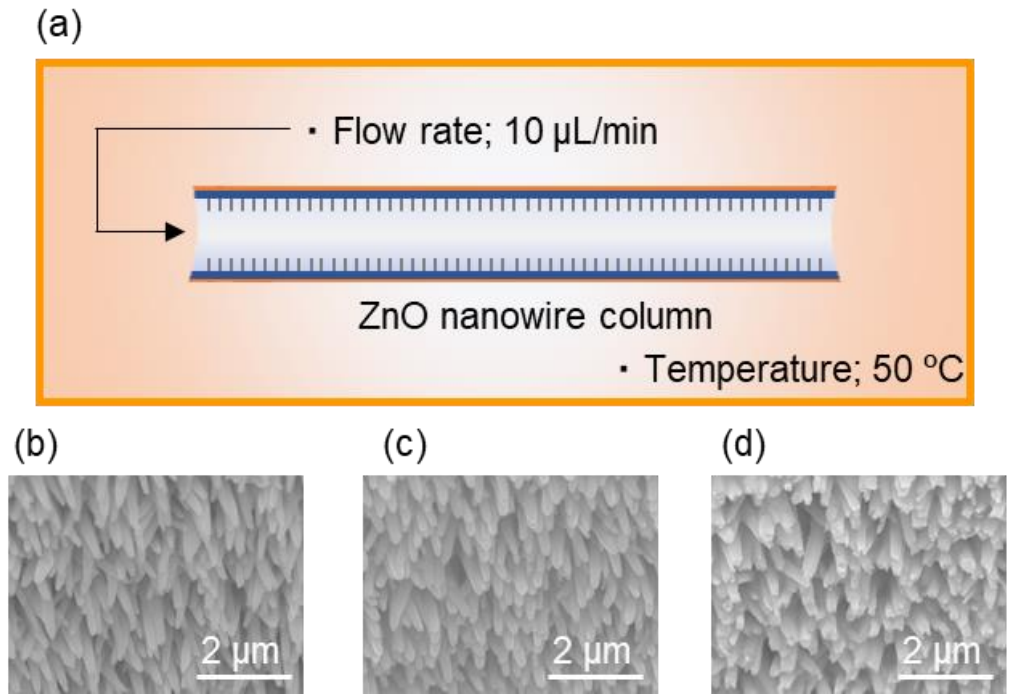

Figure S6. Physical damage test of the ZnO NWs after LC analysis. (a) Schematic diagram of physical damage test. (b) SEM image of ZnO NWs before LC analysis. (c) SEM image of ZnO NWs after LC analysis at high flow rate of 10 μL/min, (c) SEM image of ZnO NWs after LC analysis at 50 °C.

4.6 Separation of phosphorylated nucleotides by gradient elution

Nucleotides could be adsorbed on ZnO NWs via the ionic electrostatic interaction of their phosphate groups. Eqn (1) indicates that the electrostatic interaction is strongly influenced by the dielectric constant of the solvent. Hence, the competitive coordination of salts or decreasing the dielectric constant in the electrolyte solutions may tune the adsorption of nucleotides. For

the collection of adsorbed nucleotides on ZnO NWs, we evaluated the retention behaviors of ATP in different electrolyte solutions such as a NaCl solution, tris(hydroxymethyl) aminomethane-HCl (Tris–HCl buffer), and phosphate buffer. Fig. S7† shows the recovery ratios of ATP in the different electrolyte solutions. For each electrolyte solution, the ionic strength was standardized to 0.2 M. Unexpectedly, the recovery ratios of ATP did not increase in the NaCl solution or the Tris– HCl buffer. On the other hand, the recovery ratio of ATP significantly increased in the phosphate buffer. These observations may be due to the stronger coordination of the phosphate groups to Zn^{2+} than any other monovalent ions. Thus, the adsorption of nucleotides can be controlled by the competitive coordination of phosphate ions in the mobile phase due to their same charge.

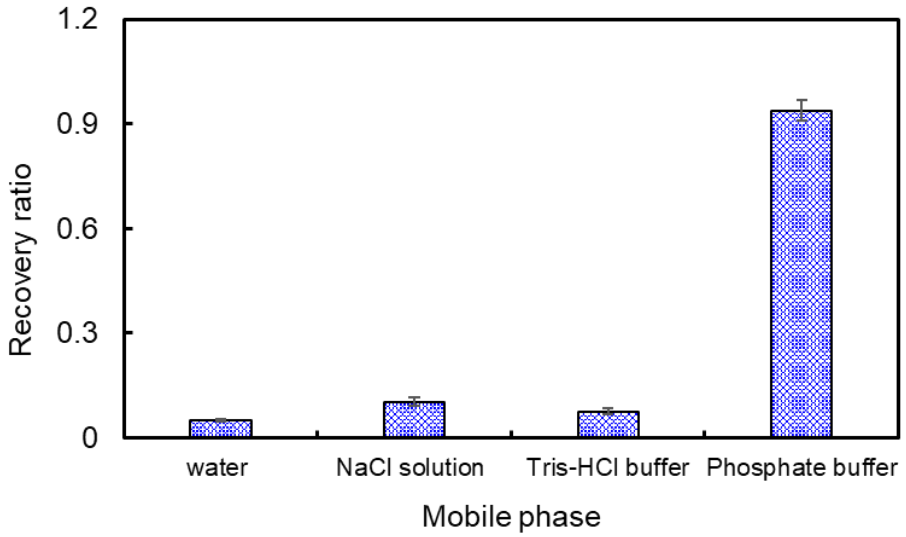

Figure S7. Recovery ratio of ATP in each electrolyte solution as the mobile phase. LC condition: column, ZnO-NWs (30 cm × 100 μm), bare capillary (30 cm × 100 μm); mobile phase, NaCl solution, Tris-HCl buffer and phosphate buffer; flow rate, 5.0 μL/min; temperature, 25 °C; detection, UV (260 nm).

Finally, we investigated the effectiveness of the phosphate-gradient condition to separate the nucleotides. As expected, AMP, ADP, and ATP were eluted from the ZnO-NW column in this order as the concentration of the phosphate ions increased in the mobile phase. However, ADP and ATP were not sufficiently separated due to the much lower plate number of the column, which is an index of the column efficiency. Briefly, the 30 cm ZnO-NW column was not long enough for sufficient separation (Fig. S8†). Increasing the length of the ZnO-NW column achieved a more effective separation because a longer column can generate enough plate numbers to distinguish between the neighboring peaks.[69]

We prepared a 90 cm ZnO-NW column (meter-long ZnO-NW column) using the flow-assisted method.[40] Fig. 6 shows chromatograms for a mixture of nucleotides. As expected, the nucleotides were successfully separated. Furthermore, the change in the back pressure was negligible on the meter-long ZnO-NW column (3.1 MPa) compared with the shorter column (0.4 MPa) due to the lower packing rate. This value was much lower than that in a typical silica-based monolithic column (15 cm, 21.1 MPa) under the same conditions. Therefore, the meter-long ZnO-NW column may realize a novel separation medium for low back pressure and robust biomolecular analysis with unique phosphate recognition. In the present situation, the gradient separation slightly dissolved the ZnO NWs, and the same column could not provide a reproducible separation. The dissolutions of ZnO NWs were not confirmed with NaCl or Tris-buffer. Thus, the chemical robustness toward the phosphate buffer may be low due to the high affinity to the phosphoric groups. To realize a practical separation media, the chemical robustness toward the phosphate buffer should be improved in the future. For example, thermal annealing treatment is effective for increasing the crystallization and improving the stability of ZnO nanowires.[70,71] Then, we compared the stabilities of the annealed nanowires (350 °C, 1 h) and as-grown nanowires in phosphate buffer. The stability of the annealed nanowires was clearly improved and the morphology is maintained after immersing into phosphate buffer for 5 hours, even though the as-grown nanowires gradually change their morphology and dissolve completely after 5 hours.

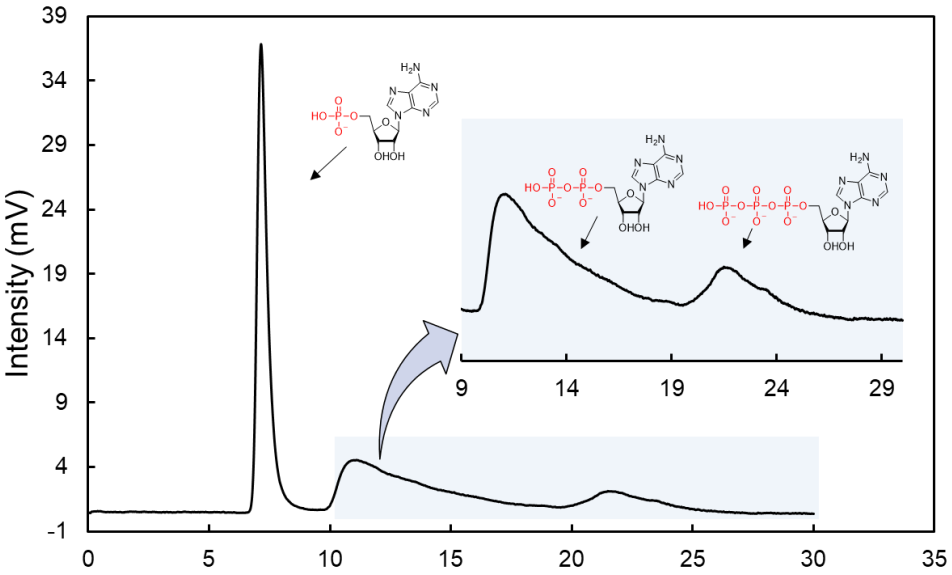

Figure S8. Chromatogram of nucleotides with the meter-long ZnO NWs column with phosphate gradient condition. LC conditions: Column, ZnO NWs column (90 cm × 100 μm); Mobile phase, (A) water, (B) 250 mM phosphate buffer; 0-1 min, 0% B, 1-21 min 0% B to 100% B, 21-30 min 100% B; flow rate, 1.0 μL/min; temperature 25 °C; detection, UV (260 nm).

4.7 References

[1] M. Stengel, D. Vanderbilt and N. A. Spaldin, Nat. Mater., 2009, 8, 392–397.

[2] H. Y. Hwang, Y. Iwasa, M. Kawasaki, B. Keimer, N. Nagaosa and Y. Tokura, Nat. Mater., 2012, 11, 103–113.

[3] N. C. Bristowe, J. Varignon, D. Fontaine, E. Bousquet and P. Ghosez, Nat. Commun., 2015, 6, 6677.

[4] W. M. Li, J. F. Zhao, L. P. Cao, Z. Hu, Q. Z. Huang, X. C. Wang, Y. Liu, G. Q. Zhao, J. Zhang, Q. Q. Liu, R. Z. Yu, Y. W. Long, H. Wu, H. J. Lin, C. T. Chen, Z. Li, Z. Z. Gong, Z. Guguchia, J. S. Kim, G. R. Stewart, Y. J. Uemura, S. Uchida and C. Q. Jin, Proc. Natl. Acad. Sci. U. S. A., 2019, 116, 12156.

[5] S. Zhang, H. Vo and G. Galli, Chem. Mater., 2021, 33, 3187– 3195.

[6] E. J. Braham, D. Sellers, E. Emmons, R. Villarreal, H. Asayesh-Ardakani, N. A. Fleer, K. E. Farley, R. Shahbazian-Yassar, R. Arr`oyave, P. J. Shamberger and S. Banerjee, Chem. Mater., 2018, 30, 214–224.

[7] T. Wang, Y. Shi, F. M. Puglisi, S. Chen, K. Zhu, Y. Zuo, X. Li, X. Jing, T. Han, B. Guo, K. Bukviˇsov´a, L. Kacht´ık, M. Kol´ıbal, C. Wen and M. Lanza, ACS Appl. Mater. Interfaces, 2020, 12, 11806–11814.

[8] A. Pucci, M.-G. Willinger, F. Liu, X. Zeng, V. Rebuttini, G. Clavel, X. Bai, G. Ungar and N. Pinna, ACS Nano, 2012, 6, 4382–4391.

[9] G. Guo, L. Ji, X. Shen, B. Wang, H. Li, J. Hu, D. Yang and A. Dong, J. Mater. Chem. A, 2016, 4, 16128–16135.

[10] F. Ji, X. Ren, X. Zheng, Y. Liu, L. Pang, J. Jiang and S. Liu, Nanoscale, 2016, 8, 8696–8703.

[11] X. Liu, Y. Sun, M. Yu, Y. Yin, B. Du, W. Tang, T. Jiang, B. Yang, W. Cao and M. N. R. Ashfold, Sens. Actuators, B, 2018, 255, 3384–3390.

[12] Z. Zhang, Q. Wu, G. Johnson, Y. Ye, X. Li, N. Li, M. Cui, J. D. Lee, C. Liu, S. Zhao, S. Li, A. Orlov, C. B. Murray, X. Zhang, T. B. Gunnoe, D. Su and S. Zhang, J. Am. Chem. Soc., 2019, 141, 16548–16552.

[13] H. Kloust, R. Zierold, J.-P. Merkl, C. Schmidtke, A. Feld, E. P¨oselt, A. Kornowski, K. Nielsch and H. Weller, Chem. Mater., 2015, 27, 4914–4917.

[14] V. Polshettiwar, B. Baruwati and R. S. Varma, ACS Nano, 2009, 3, 728–736.

[15] Y.-B. Hahn, R. Ahmad and N. Tripathy, Chem. Commun., 2012, 48, 10369–10385.

[16] Z. Li, H. Li, Z. Wu, M. Wang, J. Luo, H. Torun, P. Hu, C. Yang, M. Grundmann, X. Liu and Y. Fu, Mater. Horiz., 2019, 6, 470– 506.

[17] M. J. Limo, A. Sola-Rabada, E. Boix, V. Thota, Z. C. Westcott, V. Puddu and C. C. Perry, Chem. Rev., 2018, 118, 11118– 11193.

[18] M. J. Limo, A. Sola-Rabada, E. Boix, V. Thota, Z. C. Westcott, V. Puddu and C. C. Perry, Chem. Rev., 2018, 118, 11118– 11193.

[19] A. Kolmakov, D. O. Klenov, Y. Lilach, S. Stemmer and M. Moskovits, Nano Lett., 2005, 5, 667–673.

[20] W. T. Koo, S. Qiao, A. F. Ogata, G. Jha, J.-S. Jang, V. T. Chen, I.-D. Kim and R. M. Penner, ACS Nano, 2017, 11, 9276–9285.

[21] R. Janissen, P. K. Sahoo, C. A. Santos, A. M. da Silva, A. A. G. von Zuben, D. E. P. Souto, A. D. T. Costa, P. Celedon, N. I. T. Zanchin, D. B. Almeida, D. S. Oliveira, L. T. Kubota, C. L. Cesar, A. P. d. Souza and M. A. Cotta, Nano Lett., 2017, 17, 5938–5949.

[22] M. Chen, L. Mu, S. Wang, X. Cao, S. Liang, Y. Wang, G. She, J. Yang, Y. Wang and W. Shi, ACS Chem. Neurosci., 2020, 11, 1283–1290.

[23] Y. Li, F. Qian, J. Xiang and C. M. Lieber, Mater. Today, 2006, 9, 18–27.

[24] H. S. Jung, Y. J. Hong, Y. Li, J. Cho, Y.-J. Kim and G.-C. Yi, ACS Nano, 2008, 2, 637–642.

[25] P. Tongying, F. Vietmeyer, D. Aleksiuk, G. J. Ferraudi, G. Krylova and M. Kuno,

Nanoscale, 2014, 6, 4117–4124.

[26] X. Zhao, K. Nagashima, G. Zhang, T. Hosomi, H. Yoshida, Y. Akihiro, M. Kanai, W. Mizukami, Z. Zhu, T. Takahashi, M. Suzuki, B. Samransuksamer, G. Meng, T. Yasui, Y. Aoki, Y. Baba and T. Yanagida, Nano Lett., 2020, 20, 599–605.

[27] P. Sharma, H. A. Cho, J.-W. Lee, W. S. Ham, B. C. Park, N.-H. Cho and Y. K. Kim, Nanoscale, 2017, 9, 15371–15378.

[28] Z. Li, R. Yang, M. Yu, F. Bai, C. Li and Z. L. Wang, J. Phys. Chem. C, 2008, 112, 20114–20117.

[29] J. Zhou, N. S. Xu and Z. L. Wang, Adv. Mater., 2006, 18, 2432– 2435.

[30] Y. Wang, Y. Wu, F. Quadri, J. D. Prox and L. Guo, Nanomaterials, 2017, 7(4), 80.

[31] C. Wang, T. Hosomi, K. Nagashima, T. Takahashi, G. Zhang, M. Kanai, H. Yoshida and T. Yanagida, ACS Appl. Mater. Interfaces, 2020, 12, 44265–44272.

[32] R. Yu, C. Pan and Z. L. Wang, Energy Environ. Sci., 2013, 6, 494–499.

[33] T. Yasui, T. Yanagida, S. Ito, Y. Konakade, D. Takeshita, T. Naganawa, K. Nagashima, T. Shimada, N. Kaji, Y. Nakamura, I. A. Thiodorus, Y. He, S. Rahong, M. Kanai, H. Yukawa, T. Ochiya, T. Kawai and Y. Baba, Sci. Adv., 2017, 3, e1701133.

[34] T. Kubo, Y. Murakami, M. Tsuzuki, H. Kobayashi, T. Naito, T. Sano, M. Yan and K. Otsuka, Chem.–Eur. J., 2015, 21, 18095–18098.

[35] T. Kubo, E. Kanao, T. Matsumoto, T. Naito, T. Sano, M. Yan and K. Otsuka, ChemistrySelect, 2016, 1, 5900–5904.

[36] E. Kanao, T. Kubo, T. Naito, T. Matsumoto, T. Sano, M. Yan and K. Otsuka, J. Phys. Chem. C, 2018, 122, 15026–15032.

[37] E. Kanao, T. Kubo, T. Naito, T. Sano, M. Yan, N. Tanaka and K. Otsuka, Anal. Chem., 2020, 92, 4065–4072.

[38] E. Kanao, T. Kubo, T. Naito, T. Matsumoto, T. Sano, M. Yan and K. Otsuka, Anal. Chem., 2019, 91, 2439–2446.

[39] E. Kanao, T. Morinaga, T. Kubo, T. Naito, T. Matsumoto, T. Sano, H. Maki, M. Yan and K. Otsuka, Chem. Sci., 2020, 11, 409–418.

[40] R. Kamei, T. Hosomi, E. Kanao, M. Kanai, K. Nagashima, T. Takahashi, G. Zhang, T. Yasui, J. Terao, K. Otsuka, Y. Baba, T. Kubo and T. Yanagida, ACS Appl. Mater. Interfaces, 2021, 13, 16812–16819.

[41] D. G. Hardie, F. A. Ross and S. A. Hawley, Nat. Rev. Mol. Cell Biol., 2012, 13, 251–262.

[42] C. Bressan, A. Pecora, D. Gagnon, M. Snapyan, S. Labrecque, P. De Koninck, M. Parent and A. Saghatelyan, eLife, 2020, 9, e56006.

[43] B. Li, S.-X. Dou, J.-W. Yuan, Y.-R. Liu, W. Li, F. Ye, P.-Y. Wang and H. Li, Proc. Natl. Acad. Sci. U. S. A., 2018, 115, 12118.

[44] K. Y. Hara and A. Kondo, Microb. Cell Fact., 2015, 14, 198.

[45] H. Ghannam, A. Chahboun and M. Turmine, RSC Adv., 2019, 9, 38289–38297.

[46] S. L. Cheng, J. H. Syu, S. Y. Liao, C. F. Lin and P. Y. Yeh, RSC Adv., 2015, 5, 67752–67758.

[47] T. Shimada, T. Yasui, A. Yonese, T. Yanagida, N. Kaji, M. Kanai, K. Nagashima, T. Kawai and Y. Baba, Micromachines, 2020, 11, 610.

[48] L. Cao, J. Kiely, M. Piano and R. Luxton, Sci. Rep., 2018, 8, 12687.

[49] V. Gerbreders, M. Krasovska, I. Mihailova, A. Ogurcovs, E. Sledevskis, A. Gerbreders, E. Tamanis, I. Kokina and I. Plaksenkova, Sens. Bio-Sens. Res., 2019, 23, 100276.

[50] A. Dom´ınguez, S. grosse Holthaus, S. K¨oppen, T. Frauenheim and A. L. da Rosa, Phys. Chem. Chem. Phys., 2014, 16, 8509–8514.

[51] L. G. Gagliardi, C. B. Castells, C. R`afols, M. Ros´es and E. Bosch, J. Chem. Eng. Data, 2007, 52, 1103–1107.

[52] L. Liu, G. Duclos, B. Sun, J. Lee, A. Wu, Y. Kam, E. D. Sontag, H. A. Stone, J. C. Sturm, R. A. Gatenby and R. H. Austin, Proc. Natl. Acad. Sci. U. S. A., 2013, 110, 1686.

[53] H.-X. Yuan, Y. Xiong and K.-L. Guan, Mol. Cell, 2013, 49, 379– 387.

[54] U. Olsson and M. Wolf-Watz, Nat. Commun., 2010, 1, 111.

[55] C. Zhang, Z. Liu, X. Liu, L. Wei, Y. Liu, J. Yu and L. Sun, Acta Pharm. Sin. B, 2013, 3, 254–262.

[56] K. Ariga, H. Ito, J. P. Hill and H. Tsukube, Chem. Soc. Rev., 2012, 41, 5800–5835.

[57] A. A. Ahmed, S. Gypser, P. Leinweber, D. Freese and O. Kuhn, ¨ Phys. Chem. Chem. Phys., 2019, 21, 4421–4434.

[58] M. Yaguchi, T. Uchida, K. Motobayashi and M. Osawa, J. Phys. Chem. Lett., 2016, 7, 3097–3102.

[59] C. Wang, T. Hosomi, K. Nagashima, T. Takahashi, G. Zhang, M. Kanai, H. Zeng, W. Mizukami, N. Shioya, T. Shimoaka, T. Tamaoka, H. Yoshida, S. Takeda, T. Yasui, Y. Baba, Y. Aoki, J. Terao, T. Hasegawa and T. Yanagida, Nano Lett., 2019, 19, 2443–2449.

[60] J. Joo, B. Y. Chow, M. Prakash, E. S. Boyden and J. M. Jacobson, Nat. Mater., 2011, 10, 596–601.

[61] B. Saravanakumar and S.-J. Kim, J. Phys. Chem. C, 2014, 118, 8831–8836.

[62] T.-P. Chen, S.-P. Chang, F.-Y. Hung, S.-J. Chang, Z.-S. Hu and K.-J. Chen, Sensors, 2013, 13, 3941–3950.

[63] J. Liu, K. Nagashima, H. Yamashita, W. Mizukami, J. Uzuhashi, T. Hosomi, M. Kanai, X. Zhao, Y. Miura, G. Zhang, T. Takahashi, M. Suzuki, D. Sakai, B. Samransuksamer, Y. He, T. Ohkubo, T. Yasui, Y. Aoki, J. C. Ho, Y. Baba and T. Yanagida, Commun. Mater., 2020, 1, 58.

[64] K. Sun, H.-Y. Su and W.-X. Li, Theor. Chem. Acc., 2013, 133, 1427.

[65] S. Akhter, K. Lui and H. H. Kung, J. Phys. Chem., 1985, 89, 1958–1964.

[66] D. Mora-Fonz, T. Lazauskas, M. R. Farrow, C. R. A. Catlow, S. M. Woodley and A. A. Sokol, Chem. Mater., 2017, 29, 5306–5320.

[67] T. Enomoto, Y. Nakamori, K. Matsumoto and R. Hagiwara, J. Phys. Chem. C, 2011, 115, 4324–4332.

[68] M. Kohagen, E. Pluha˘rov´a, P. E. Mason and P. Jungwirth, J. Phys. Chem. Lett., 2015, 6, 1563–1567.

[69] H. G. Barth, LC GC N. Am., 2018, 36, 830–835.

[70] K. Nakamura, T. Takahashi, T. Hosomi, T. Seki, M. Kanai, G. Zhang, K. Nagashima, N. Shibata and T. Yanagida, ACS Appl. Mater. Interfaces, 2019, 11, 40260–40266.

[71] O. Lupan, N. Magariu, R. Khaledialidusti, A. K. Mishra, S. Hansen, H. Kruger, V. Postica, H. Heinrich, B. Viana, ¨ L. K. Ono, B. R. Cuenya, L. Chow, R. Adelung and T. Pauport´e, ACS Appl. Mater. Interfaces, 2021, 13, 10537– 10552.

Chapter V

Rational Strategy for Space-Confined Atomic Layer Deposition

5.1 Introduction

Decorating artificially inner surface properties of confined spaces offers an interesting approach to design novel chemical events within spaces.[1–7] An interaction between molecules and surrounding inner surfaces clearly dominates phenomena within confined spaces.[8–13] Although there are various surface decoration methods for inner surfaces of confined spaces,[14–16] inorganic solid decorations are particularly interesting candidates due to their thermal and chemical robustness and the elemental variation, which are hardly attainable to conventional organic surface modifications.[8,17,18] Among various inorganic solid surface decoration methods, atomic layer deposition (ALD) is one of powerful deposition techniques because of the excellent spatial deposition uniformity and atomic layer level thickness controllability even for complex nanostructured surfaces including needled like high-aspect ratio nanostructures, which are hardly attainable to other conventional deposition methods.[19–35] In conventional ALD processes, the objects and/or targets to be deposited have been mostly various shaped substrates in open-top circumstances,[19,20] rather than the inner surface of confined spaces. Therefore, commercially available various ALD systems have been designed to operate under such open-top environments, where introducing precursors and/or waters into ALD chambers is easily performed without adding any special structures due to the relatively high flow conductance.[22] In principle of ALD, supplying and/or removing precursors (or waters) on surfaces are critical processes to appropriately perform depositions.[26] Inherently, such supply

and removal of precursors tends to be more difficult for confined spaces especially at high aspect ratios.[23] This is because the flow conductance for exchanging precursors tends to decrease as increasing the aspect ratio of confined spaces.[36] Although the application of unique ALD techniques to confined spaces is clearly fascinating for designing chemical events within spaces, above inherent limitation of ALD hinders conventional ALD methodologies from performing depositions for inner surfaces of confined spaces. Here we propose a rational methodology to overcome above difficulty of ALD for confined spaces. We design own ALD systems, which can generate differential pressures to confined spaces. This ALD system enables us to successfully deposit TiOx layer onto the inner surface of capillary tubes with the length of 1000 mm and the inner diameter of 100 μm, where conventional ALD methods are not applicable. Furthermore, we show the superior thermal and chemical robustness of such TiOx-coated capillary tubes for molecular separations when compared to conventional molecular coated capillary tubes.

5.1 In-tube ALD growth by conventional method

Figure 1 (a) illustrates the schematic of experimental systems employed for conventional ALD. Microtubes with various inner diameters: ID (ranged from 0.5 mm to 2 mm) and the length of 100 mm were placed into the ALD chamber. Ti precursor (TMA) was used for these depositions. The deposition temperature was 150 °C. Figure 1(b) shows the spatial uniformity of TiO_x depositions onto the inner surfaces of microtubes when varying the size of inner diameter. Since it is difficult to directly measure the TiO_x thin film thickness on the inner wall of microtubes with the length of 100 mm, we performed EDS measurements on the inner wall to measure the deposited Ti amount. Glass microtube was cut at several points and their EDS spectra at cross-sectional images were measured. The EDS intensity ratio of Si (component of microtube body) and Ti was extracted as the index of spatial deposition uniformity, as shown in Figure 1(b). As clearly seen in Figure 1(b), there is a significant size effect of inner diameter (ID) on the the spatial uniformity of TiO_x depositions. In the case of microtube with the inner diameter of 2 mm, the TiO_x deposition was spatially uniform over the microtube length of 100 mm. However, such deposition uniformity tends to deteriorate as the inner diameter decreases. For the inner diameter of 1 mm, the TiO_x could be deposited only near both edges of microtubes, but not for the center part. When the inner diameter was smaller than 0.5 mm, the TiO_x could not be deposited at all for entire microtubes. Figure 1c shows the comparison between

previously reports and the present data on ALD growth data within microtubes when varying the inner diameter and the length.[1,37–39] As seen in the figure, the ALD depositable geometry of microtubes in previous works is consistent with the present data. The reason why there is a difficulty to perform ALD growth within microtubes is clearly related to the low flow conductance of capillary microtubes, *i.e.* the supplied precursors cannot reach the center part of microtubes. Thus, there is an inherent limitation of conventional ALD methodology to deposit the inner surfaces of microtubes, where the space confinement effect dominates.

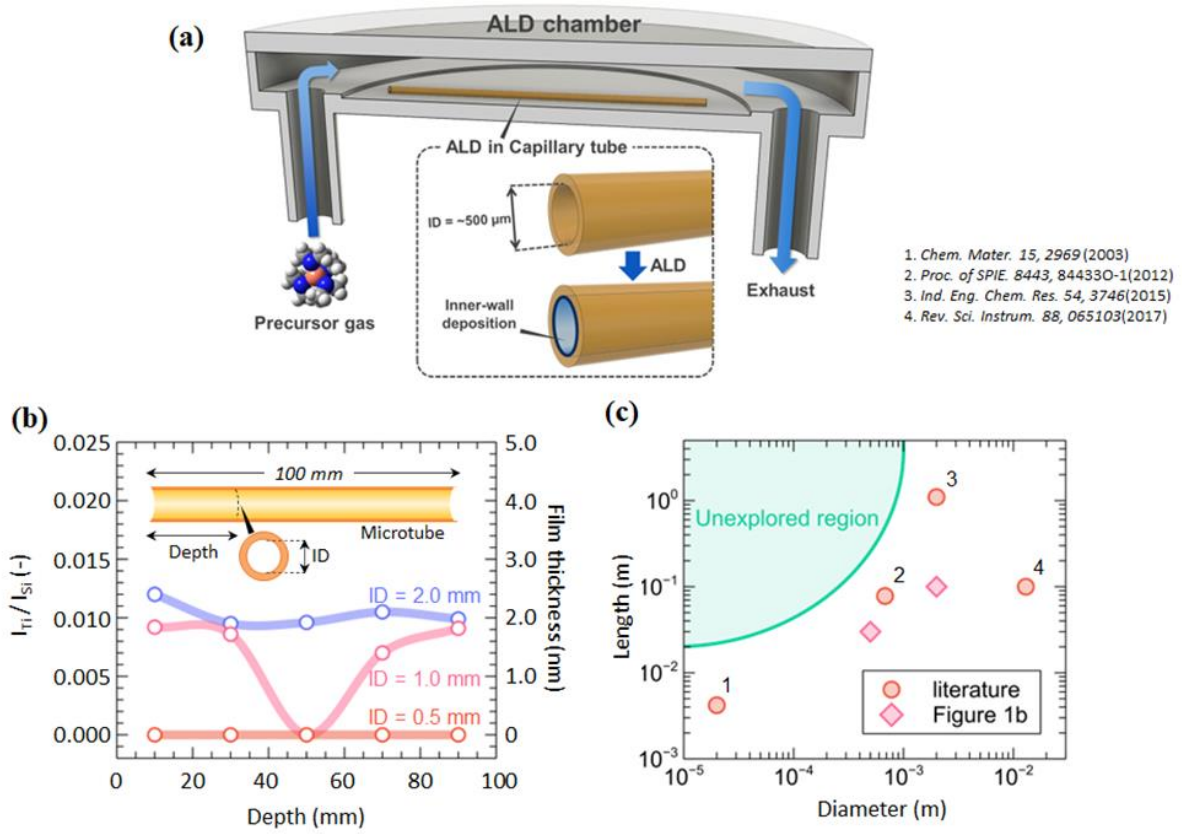

Figure 1. (a) Schematic of typical ALD system employed, (b) Spatial uniformity data of TiOx depositions by conventional ALD system onto the inner surface of microtubes when varying

inner diameters, and the relative EDS intensity ratio of Ti/Si (ITi / ISi) and the deposition thickness were shown, (c) Comparison between the present data and previous data [1: Chem. Mater. 15, 2969 (2003), 2: Proc. of SPIE. 8443, 84433O-1(2012), 3: Ind. Eng. Chem. Res. 54, 3746 (2015), 4: Rev. Sci. Instrum. 88, 065103 (2017)] on the depositable geometry of microtubes by conventional ALD.

5.2 Limitation of precursor delivery to microtubes

Conventional ALD processes for film depositions are performed in the presence of flows to deliver precursors and/or waters onto the target surfaces. However, as illustrated in Figure 2a, the necessity of such flow process inherently limits the precursor supply into confined spaces like microtubes. This is because the flow conductance of microtubes tends to decrease as the inner diameter decreases, and a diffusion of precursors dominates the total precursor transportation. Based on Arnold's formula,[37] a diffusion is inverse proportional to pressure (Equation: $D=0.00837T^{3/2}(1/M_1+1/M_2)^{1/2}/P(V_{b1}^{1/3}+V_{b2}^{1/3})^2(1+S_{12}/T)$). Thus, within the framework of diffusion-rate determining processes, depositing at lower pressures is required to enhance the deposition rate via increased diffusion constant. However, for microtubes, a precursor supply only via diffusion requires an extremely long time (*e.g.*, estimated to be 3700 sec for the length of 100 mm and the inner diameter of 100 μm: See the calculation details in Supplementary Information), which is clearly not realistic time range for experiments. One

possible strategy to overcome this issue is to utilize differential pressures across microtubes, generating a forced flow. As shown in Figure 2b, we calculate the molecule arrival time through the microtubes as a function of differential pressures when varying the inner diameter of microtubes. See the calculation details in Supplementary Information. For example, in the microtubes with the inner diameters (100 μm), the differential pressures are required to be above around 500 Pa to generate a forced flow in the realistic deposition time range. Thus, it is necessary to apply the differential pressures across microtubes when both supplying precursors into microtubes and evacuating them from microtubes. However, such experimental procedures are not feasible for conventional ALD systems. We have developed the ALD system, which is capable of depositing for confined spaces like microtubes with the low flow conductance.

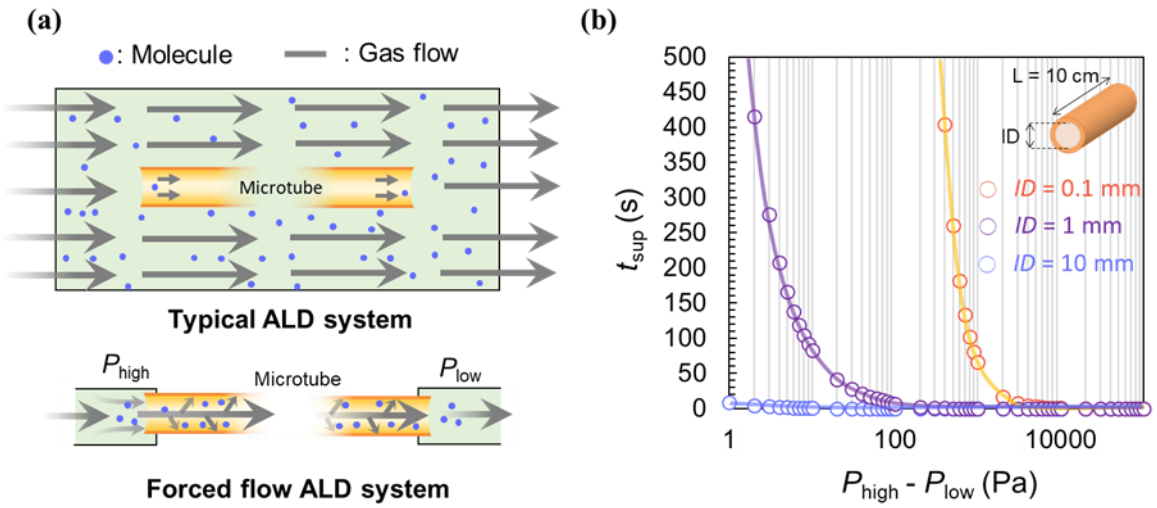

Figure 2. (a) Schematic of molecular behaviors into microtubes in typical ALD systems and/or in the forced-flow system proposed in this study, (b) Estimated molecular supply time tsup of

a microtube for various inner diameters (ID = 0.1, 1, or 10mm) plotted against differential pressures (Phigh - Plow) of inside and outside of the tube. The molecular supply time tsup is defined as the time to transport the number of precursor molecules required to form a monolayer on the inner wall of the microtubes.

5.3 New ALD and process development

Figure 3a shows the schematic of newly developed ALD system. In this system and the experimental procedures, it is designed to apply the required differential pressures across microtubes during both processes including supplying precursors into microtubes and removing them from microtubes. As illustrated in Figure 3a, the pressure at both ends of the capillary tube can be independently controlled by valve operations, and relatively large differential pressures about 10^4 Pa can be generated for the microtube. The processes for one ALD cycle consist of 6 steps, as illustrated in Figure 3b. The first process (Step 1) is a whole evacuation of all ALD chamber components. The background pressure values are typically around 0.5 Pa. In Step 2, N_2 gas mixed with precursors is filled into piping surrounding microtubes. In next Step 3, by opening two values (V2 and V3), N_2 gas mixed with precursors is fully introduced from both ends of microtubes via the generated differential pressure. After this precursor deposition onto the inner surface of microtube (Step 3), residual precursors must be removed before the next precursor supply. In Step 4, by opening three valves (V2, V3 and

V4), residual N_2 gas mixed with precursors is evacuated from all piping surrounding microtube. However, due to the low flow conductance of microtube, it is impossible to completely remove the residual precursor gas from the microtube, as illustrated in Figure 3b. To fully evacuate the residual precursors from microtube, in Step 5, pure N_2 gas is introduced into surrounding piping by opening two valves (V1 and V2). Note that one side piping of microtube near valve (V3) is intentionally closed to keep low pressure level (0.5 Pa). And then in Step 6, by opening two valves (V3 and V4), the residual precursors can be completely moved from microtubes by the N_2 forced flow via the pre-generated differential pressure. Thus, by utilizing the differential pressures across microtubes, supplying and/or evacuating precursors into/from microtube can be performed for ALD processes. Note that these experimental procedures utilizing differential pressures are essential to perform ALD growths for any confined spaces.

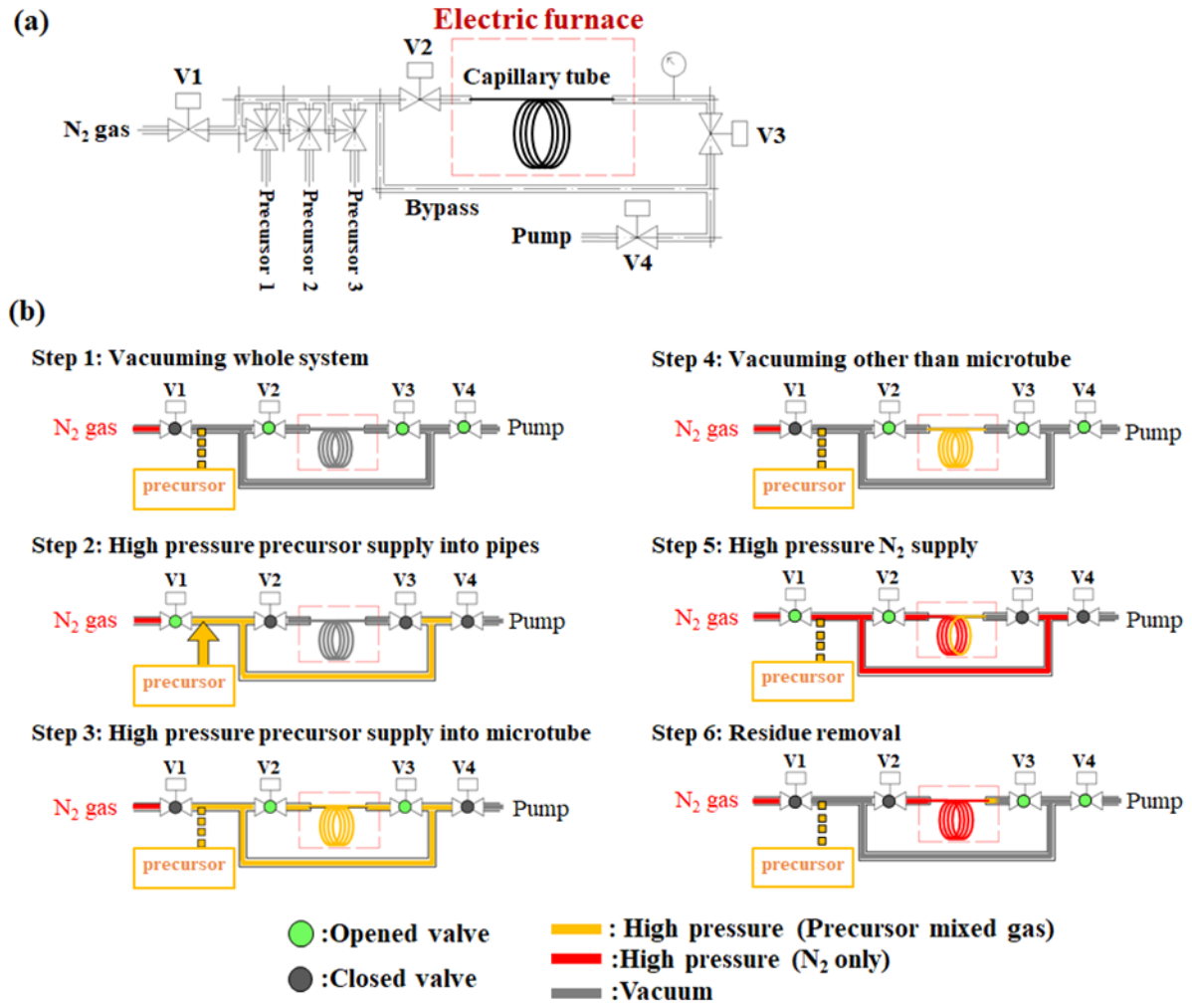

Figure 3. (a) Schematic of the developed ALD system, which can generate differential pressures for a forced-flow, (b) Schematic of proposed ALD cycles and 6 steps to perform material supply and material removal for confined microtubes.

5.4 Growth into microtubes using new ALD

Figure 4 shows the successful application of developed ALD procedures to deposit TiO_x (precursor: TDMAT) onto the inner surface of microtube with the inner diameter of 100 μm and the length of 1000 mm (the aspect ratio: 10000). Figure 4a shows the photograph of

employed whole capillary microtube, and the measurements for deposition uniformity were performed at various positions A-J. Figure 4b shows the comparison between the developed ALD (High Differential Pressure ALD) and conventional ALD on the TiO_x deposition onto the inner surface of microtubes. The y-axis values of TiO_x deposition thickness were calculated from the correlation between EDS intensity and film thickness, which was obtained for TiO_x films on flat SiO_x substrate. Typically, EDS intensity ratio (Ti/Si) of 0.02 corresponds to TiO_x thickness of 0.4 nm. As clearly seen in Figure 4b, the sample prepared by conventional ALD system did not show any TiO_x growth in the microtube. On the other hands, spatially uniform TiO_x deposition can be seen for sample prepared by newly developed ALD system. These results highlight that our developed ALD system enables to perform uniform growths on the inner surface wall of long capillary microtube with the inner diameter of 100 μm and the length of 1000 mm. Note that any previous ALD systems are not capable of depositing for such capillary microtubes.

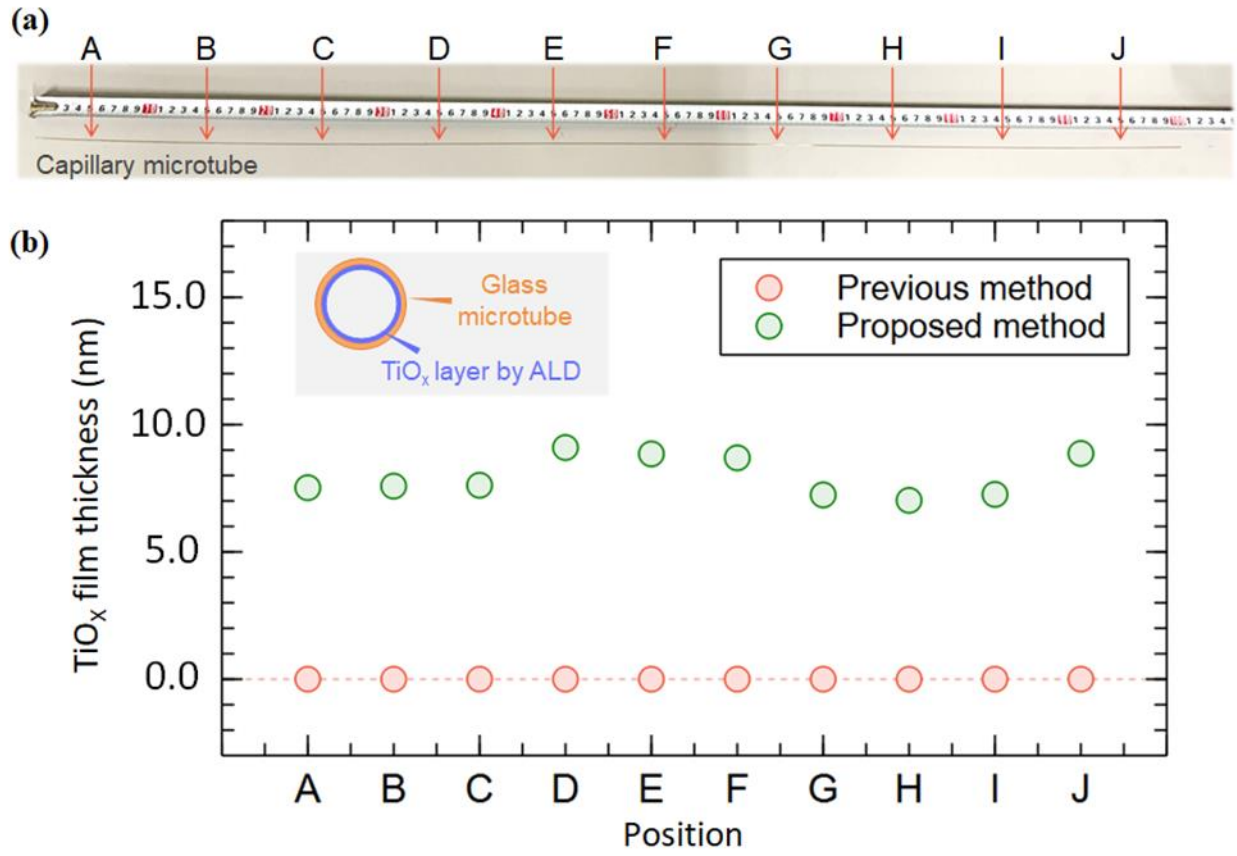

Figure 4. (a) Photograph of a capillary microtube. the spatial locations measured for EDS were highlighted as A-J, (b) Spatial uniformity of TiOx deposition on the inner surfaces at various positions of microtube.

5.5 Applications of ALD-modified microtubes

Figure Finally, we examine the applicability of fabricated capillary microtubes with TiO_x on the inner surface for thermally robust gas chromatography, as illustrated in Figure 5a. Figure 5b shows the comparison between the present capillary microtubes with TiO_x and conventional molecular decorated InertCap FFAP capillary column on the retention data using

the carboxylic acids (nonanoic acid, hexanoic acid). To examine the thermal robustness, we measured the thermal durability of both capillary columns in the Figure. Figure 5c summarizes the thermal durability of retention time when varying the thermal cycling time. As seen in the Figure, the present capillary microtubes with TiO_x on the inner surface exhibited the superior thermal stability when compared with the conventional FFAP capillary column. As the cycle number of thermal endurance increased, the retention time of FFAP significantly decreased, whereas the retention time of the present capillary microtubes with TiO_x could be maintained. Thus, the present capillary column coated by TiO_x via ALD can separate highly polar molecules with the thermally robustness, which had been relatively difficult using conventional molecular coted capillary columns. Furthermore, our ALD method could be applied to the nanostructure formed in microtubes. We have previously constructed ZnO nanowires (ZnO-NW) on the inner wall of microtube capillary and implemented the capillary as a liquid phase separation column; the ZnO-NWs could adsorb phosphonic acids via electrostatic interaction.[40,41] However, the corrosion morphology of ZnO-NWs in the capillary column was confirmed after exposure to acetate buffer in 4 h (Figure 4 (d), (e)), and this corrosion led to a loss of adsorption capacity for phosphonic acid (See the details in Supporting Information). In contrast, ZnO-NWs coated by TiOx via ALD could keep their specific adsorption capacity for phosphonic acids without corrosion of their inner-nanowire structures (Figure 4 (e)). Briefly, the TiOx coating via ALD improved the chemical robustness as a separation media of ZnO-NWs. Since this capillary

column application is just an example of various applications of the proposed ALD system to decorate the inner surface of confined spaces, the present rational strategy of space-confined ALD offers a unique approach to design chemical and physical properties of various confined spaces.

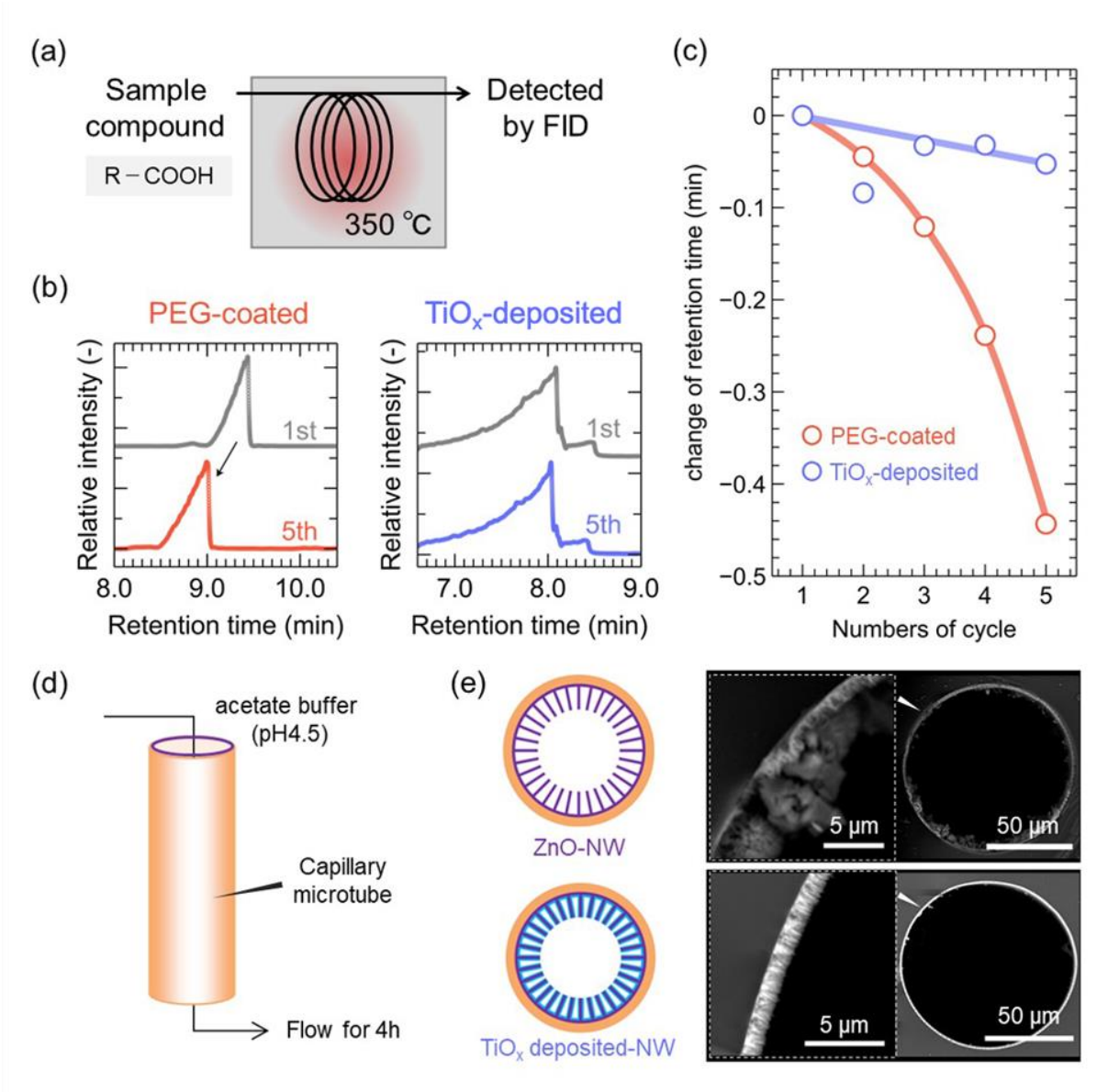

Figure5. (a) Overview of molecular separation experiments with ALD-deposited microtubes used as GC column. (b) Change in carboxylic acids peak retention time after five measurements on a PEG-coated column (left) and a TiO_x-deposited column (right). (c) A schematic image of liquid-phase leaching resistance tests. 10 mM acetate buffer (pH 4.5) was used as the liquid phase. (d) Overview of . (e) SEM images of a ZnO nanowire-arrayed capillary microtube (bare-NW) and a TiO_x-deposited ZnO nanowire-arrayed capillary microtube (TiO_x-deposited) after soaked with acetate buffer solution for 4 h.

5.6 References

[1] Becker, J. S.; Suh, S.; Wang, S.; Gordon, R. G. Highly Conformal Thin Films of Tungsten Nitride Prepared by Atomic Layer Deposition from a Novel Precursor. *Chem. Mater.* **2003**, *15* (15), 2969–2976. https://doi.org/10.1021/cm021772s.

[2] Daiguji, H.; Yang, P.; Majumdar, A. Ion Transport in Nanofluidic Channels. *Nano Lett.* **2004**, *4* (1), 137–142. https://doi.org/10.1021/nl0348185.

[3] Green, Y.; Eshel, R.; Park, S.; Yossifon, G. Interplay between Nanochannel and Microchannel Resistances. *Nano Lett.* **2016**, *16* (4), 2744–2748. https://doi.org/10.1021/acs.nanolett.6b00429.

[4] Wang, M.; Cheng, B.; Yang, Y.; Liu, H.; Huang, G.; Han, L.; Li, F.; Xu, F. Microchannel Stiffness and Confinement Jointly Induce the Mesenchymal-Amoeboid Transition of Cancer Cell Migration. *Nano Lett.* **2019**, *19* (9), 5949–5958. https://doi.org/10.1021/acs.nanolett.9b01597.

[5] Ostler, D.; Kannam, S. K.; Frascoli, F.; Daivis, P. J.; Todd, B. D. Efficiency of Electropumping in Nanochannels. *Nano Lett.* **2020**, *20* (5), 3396–3402. https://doi.org/10.1021/acs.nanolett.0c00308.

[6] Kitao, T.; Nagasaka, Y.; Karasawa, M.; Eguchi, T.; Kimizuka, N.; Ishii, K.; Yamada, T.; Uemura, T. Transcription of Chirality from Metal–Organic Framework to Polythiophene. *J. Am. Chem. Soc.* **2019**, *141* (50), 19565–19569. https://doi.org/10.1021/jacs.9b10880.

[7] Daiguji, H. Ion Transport in Nanofluidic Channels. *Chem. Soc. Rev.* **2010**, *39* (3), 901–911. https://doi.org/10.1039/b820556f.

[8] Yasui, T.; Rahong, S.; Motoyama, K.; Yanagida, T.; Wu, Q.; Kaji, N.; Kanai, M.; Doi, K.; Nagashima, K.; Tokeshi, M.; Taniguchi, M.; Kawano, S.; Kawai, T.; Baba, Y. DNA Manipulation and Separation in Sublithographic-Scale Nanowire Array. *ACS Nano* **2013**, *7* (4), 3029–3035. https://doi.org/10.1021/nn4002424.

[9] Rahong, S.; Yasui, T.; Yanagida, T.; Nagashima, K.; Kanai, M.; Klamchuen, A.; Meng, G.; He, Y.; Zhuge, F.; Kaji, N.; Kawai, T.; Baba, Y. Ultrafast and Wide Range Analysis of DNA Molecules Using Rigid Network Structure of Solid Nanowires. *Sci. Rep.* **2014**, *4*, 5252. https://doi.org/10.1038/srep05252.

[10] Wang, G.; Shi, G.; Wang, H.; Zhang, Q.; Li, Y. In Situ Functionalization of Stable 3D Nest-Like Networks in Confined Channels for Microfluidic Enrichment and Detection. *Advanced Functional Materials* **2014**, *24* (7), 1017–1026. https://doi.org/10.1002/adfm.201301936.

[11] Hu, W.; Liu, Y.; Chen, T.; Liu, Y.; Li, C. M. Hybrid ZnO Nanorod-Polymer Brush Hierarchically Nanostructured Substrate for Sensitive Antibody Microarrays. *Adv. Mater.* **2015**, *27* (1), 181–185. https://doi.org/10.1002/adma.201403712.

[12] Rahong, S.; Yasui, T.; Yanagida, T.; Nagashima, K.; Kanai, M.; Meng, G.; He, Y.; Zhuge, F.; Kaji, N.; Kawai, T.; Baba, Y. Three-Dimensional Nanowire Structures for Ultra-Fast Separation of DNA, Protein and RNA Molecules. *Sci. Rep.* **2015**, *5*, 10584. https://doi.org/10.1038/srep10584.

[13] Zhao, D.; Wu, Z.; Yu, J.; Wang, H.; Li, Y.; Duan, Y. Highly Sensitive Microfluidic Detection of Carcinoembryonic Antigen via a Synergetic Fluorescence Enhancement Strategy Based on the Micro/Nanostructure Optimization of ZnO Nanorod Arrays and in Situ ZIF-8 Coating. *Chemical Engineering Journal* **2020**, *383*, 123230. https://doi.org/10.1016/j.cej.2019.123230.

[14] Primkulov, B. K.; Pahlavan, A. A.; Bourouiba, L.; Bush, J. W. M.; Juanes, R. Spin Coating of Capillary Tubes. *J. Fluid Mech.* **2020**, *886*, A30. https://doi.org/10.1017/jfm.2019.1072.

[15] Jeong, D.-H.; Xing, L.; Boutin, J.-B.; Sauret, A. Particulate Suspension Coating of Capillary Tubes. *Soft Matter* **2022**, *18* (42), 8124–8133. https://doi.org/10.1039/d2sm01211a.

[16] Jing, C.; Xiujian; Zhao; Han, J.; Zhu, K.; Liu, A.; Tao, H. A New Method of Fabricating Internally Sol–Gel Coated Capillary Tubes. *Surf. Coat. Technol.* **2003**, *162* (2), 228–233. https://doi.org/10.1016/S0257-8972(02)00568-6.

[17] Hu, W.; Lu, Z.; Liu, Y.; Chen, T.; Zhou, X.; Li, C. M. A Portable Flow-through Fluorescent Immunoassay Lab-on-a-Chip Device Using ZnO Nanorod-Decorated Glass Capillaries. *Lab Chip* **2013**, *13* (9), 1797–1802. https://doi.org/10.1039/c3lc41382a.

[18] Wang, G.; Li, K.; Purcell, F. J.; Zhao, D.; Zhang, W.; He, Z.; Tan, S.; Tang, Z.; Wang, H.; Reichmanis, E. Three-Dimensional Clustered Nanostructures for Microfluidic Surface-Enhanced Raman Detection. *ACS Appl. Mater. Interfaces* **2016**, *8* (37), 24974–24981. https://doi.org/10.1021/acsami.6b10542.

[19] Knoops, H. C. M.; Potts, S. E.; Bol, A. A.; Kessels, W. M. M. 27 - Atomic Layer Deposition. In *Handbook of Crystal Growth (Second Edition)*; Kuech, T. F., Ed.; North-Holland: Boston, 2015; pp 1101–1134. https://doi.org/10.1016/B978-0-444-63304-0.00027-5.

[20] Cremers, V.; Puurunen, R. L.; Dendooven, J. Conformality in Atomic Layer Deposition: Current Status Overview of Analysis and Modelling. *Applied Physics Reviews* **2019**, *6* (2), 021302. https://doi.org/10.1063/1.5060967.

[21] Elias, J.; Utke, I.; Yoon, S.; Bechelany, M.; Weidenkaff, A.; Michler, J.; Philippe, L. Electrochemical Growth of ZnO Nanowires on Atomic Layer Deposition Coated Polystyrene Sphere Templates. *Electrochim. Acta* **2013**, *110*, 387–392. https://doi.org/10.1016/j.electacta.2013.04.168.

[22] Ren, Q.-H.; Zhang, Y.; Lu, H.-L.; Wang, Y.-P.; Liu, W.-J.; Ji, X.-M.; Devi, A.; Jiang, A.-Q.; Zhang, D. W. Atomic Layer Deposition of Nickel on ZnO Nanowire Arrays for High-Performance Supercapacitors. *ACS Appl. Mater. Interfaces* **2018**, *10* (1), 468–476. https://doi.org/10.1021/acsami.7b13392.

[23] Chen, H.-S.; Chen, P.-H.; Kuo, J.-L.; Hsueh, Y.-C.; Perng, T.-P. TiO_2 Hollow Fibers with Internal Interconnected Nanotubes Prepared by Atomic Layer Deposition for Improved Photocatalytic Activity. *RSC Adv.* **2014**, *4* (76), 40482–40486. https://doi.org/10.1039/c4ra06807f.

[24] Zazpe, R.; Knaut, M.; Sopha, H.; Hromadko, L.; Albert, M.; Prikryl, J.; Gärtnerová, V.; Bartha, J. W.; Macak, J. M. Atomic Layer Deposition for Coating of High Aspect Ratio TiO_2 Nanotube Layers. *Langmuir* **2016**, *32* (41), 10551–10558. https://doi.org/10.1021/acs.langmuir.6b03119.

[25] Gu, D.; Shrestha, P.; Baumgart, H.; Namkoong, G.; Abdel-Fattah, T. M. ALD Synthesis of Tube-in-Tube Nanostructures of Transition Metal Oxides by Template Replication. *ECS Trans.* **2009**, *25* (4), 191. https://doi.org/10.1149/1.3205054.

[26] George, S. M. Atomic Layer Deposition: An Overview. *Chem. Rev.* **2010**, *110* (1), 111–131. https://doi.org/10.1021/cr900056b.

[27] Gayle, A. J.; Berquist, Z. J.; Chen, Y.; Hill, A. J.; Hoffman, J. Y.; Bielinski, A. R.; Lenert, A.; Dasgupta, N. P. Tunable Atomic Layer Deposition into Ultra-High-Aspect-Ratio (>60000:1) Aerogel Monoliths Enabled by Transport Modeling. *Chemistry of Materials* **2021**, *33* (14), 5572–5583. https://doi.org/10.1021/acs.chemmater.1c00770.

[28] Su, C.-Y.; Wang, C.-C.; Hsueh, Y.-C.; Gurylev, V.; Kei, C.-C.; Perng, T.-P. Enabling High Solubility of ZnO in TiO_2 by Nanolamination of Atomic Layer Deposition. *Nanoscale* **2015**, *7* (45), 19222–19230. https://doi.org/10.1039/c5nr06264k.

[29] Becker, J. S.; Kim, E.; Gordon, R. G. Atomic Layer Deposition of Insulating Hafnium and Zirconium Nitrides. *Chemistry of Materials* **2004**, *16* (18), 3497–3501. https://doi.org/10.1021/cm049516y.

[30] Gluch, J.; Rößler, T.; Schmidt, D.; Menzel, S. B.; Albert, M.; Eckert, J. TEM Characterization of ALD Layers in Deep Trenches Using a Dedicated FIB Lamellae Preparation Method. *Thin Solid Films* **2010**, *518* (16), 4553–4555. https://doi.org/10.1016/j.tsf.2009.12.029.

[31] Ladanov, M.; Algarin-Amaris, P.; Matthews, G.; Ram, M.; Thomas, S.; Kumar, A.; Wang, J. Microfluidic Hydrothermal Growth of ZnO Nanowires over High Aspect Ratio Microstructures. *Nanotechnology* **2013**, *24* (37), 375301. https://doi.org/10.1088/0957-4484/24/37/375301.

[32] Elam, J. W.; Routkevitch, D.; Mardilovich, P. P.; George, S. M. Conformal Coating on Ultrahigh-Aspect-Ratio Nanopores of Anodic Alumina by Atomic Layer Deposition. *Chemistry of Materials* **2003**, *15* (18), 3507–3517. https://doi.org/10.1021/cm0303080.

[33] Perez, I.; Robertson, E.; Banerjee, P.; Henn-Lecordier, L.; Son, S. J.; Lee, S. B.; Rubloff, G. W. TEM-Based Metrology for HfO_2 Layers and Nanotubes Formed in Anodic

Aluminum Oxide Nanopore Structures. *Small* **2008**, *4* (8), 1223–1232. https://doi.org/10.1002/smll.200700815.

[34] Elam, J. W.; Xiong, G.; Han, C. Y.; Wang, H. H.; Birrell, J. P.; Welp, U.; Hryn, J. N.; Pellin, M. J.; Baumann, T. F.; Poco, J. F.; Satcher, J. H. Atomic Layer Deposition for the Conformal Coating of Nanoporous Materials. *J. Nanomater.* **2006**, *2006*. https://doi.org/10.1155/JNM/2006/64501.

[35] Liu, K.-I.; Kei, C.-C.; Mishra, M.; Chen, P.-H.; Liu, W.-S.; Perng, T.-P. Uniform Coating of TiO_2 on High Aspect Ratio Substrates with Complex Morphology by Vertical Forced-Flow Atomic Layer Deposition. *RSC Advances* **2017**, *7* (55), 34730–34735. https://doi.org/10.1039/c7ra04853j.

[36] Tison, S. A. Experimental Data and Theoretical Modeling of Gas Flows through Metal Capillary Leaks. *Vacuum* **1993**, *44* (11), 1171–1175. https://doi.org/10.1016/0042-207X(93)90342-8.

[37] Nolan, M.; Povey, I.; Elliot, S.; Cordero, N.; Pemble, M.; Shortt, B.; Bavdaz, M. Uniform Coating of High Aspect Ratio Surfaces through Atomic Layer Deposition. In *Space Telescopes and Instrumentation 2012: Ultraviolet to Gamma Ray*; SPIE, 2012; Vol. 8443, pp 1086–1093. https://doi.org/10.1117/12.924876.

[38] Gong, T.; Hui, L.; Zhang, J.; Sun, D.; Qin, L.; Du, Y.; Li, C.; Lu, J.; Hu, S.; Feng, H. Atomic Layer Deposition of Alumina Passivation Layers in High-Aspect-Ratio Tubular Reactors for Coke Suppression during Thermal Cracking of Hydrocarbon Fuels. *Ind. Eng. Chem. Res.* **2015**, *54* (15), 3746–3753. https://doi.org/10.1021/ie5047818.

[39] Mishra, M.; Kei, C.-C.; Yu, Y.-H.; Liu, W.-S.; Perng, T.-P. Uniform Coating of Ta_2O_5 on Vertically Aligned Substrate: A Prelude to Forced Flow Atomic Layer Deposition. *Review of Scientific Instruments* **2017**, *88* (6), 065103. https://doi.org/10.1063/1.4983805.

[40] Kanao, E.; Nakano, K.; Kamei, R.; Hosomi, T.; Ishihama, Y.; Adachi, J.; Kubo, T.; Otsuka, K.; Yanagida, T. Moderate Molecular Recognitions on ZnO M-Plane and Their Selective Capture/Release of Bio-Related Phosphoric Acids. *Nanoscale Adv* **2022**, *4* (6), 1649–1658. https://doi.org/10.1039/d1na00865j.

[41] Kamei, R.; Hosomi, T.; Kanao, E.; Kanai, M.; Nagashima, K.; Takahashi, T.; Zhang, G.; Yasui, T.; Terao, J.; Otsuka, K.; Baba, Y.; Kubo, T.; Yanagida, T. Rational Strategy for Space-Confined Seeded Growth of ZnO Nanowires in Meter-Long Microtubes. *ACS Appl. Mater. Interfaces* **2021**, *13* (14), 16812–16819. https://doi.org/10.1021/acsami.0c22709.

Chapter VI

Overall Conclusions

6.1 Overall Conclusions

Structural and chemical alterations have been made in various ways in confined spaces to bring about new chemical interactions. In recent years, sol-gel is the mainstream for chemical coating in confined spaces. Although it is possible to create nanostructures by the sol-gel method and chemically coat them, there was no modification method that could freely adjust the nanostructures or uniformly and finely control the film thickness. This paper focused on novel structural and chemical modifications to confined spaces such as microtubes.

In Chapter 1, we explained the current status and problems of structural and chemical modifications to confined spaces. Chapter I played a role as a guideline for this thesis.

Chapter 2 summarizes previous research on structural and chemical modifications to confined spaces. Based on the summarized research results, we present problems and countermeasures.

Chapter 3 summarizes a new method for fabricating ZnO nanostructures on the inner walls of microtubes.

In Chapter 4, we used the ZnO nanowire microtubes fabricated in Chapter 3 to isolate new molecules.

In Chapter 5, we created a new device for ALD in microtubes and used the properties of ALD to uniformly grow nanostructures in microtubes.

In this study, we succeeded in chemically modifying the ZnO nanostructure and inorganic material on the inner wall of the microtube, which allows us to control the film thickness at the atomic layer level, which was not possible until now.

List of Publications

Scientific Journals in This Thesis

1. (Chapter III)

   "Rational Strategy for Space-Confined Seeded Growth of ZnO Nanowires in Meter-Long Microtubes"

   R. Kamei, T. Hosomi, E. Kanao, M. Kanai, K. Nagashima, T. Takahashi, G. Zhang, T. Yasui, J. Terao, K. Otsuka, Y. Baba, T. Kubo and T. Yanagida

   ***ACS Appl. Mater. Interfaces,* 13**, 16812−16819 (2021)

2. (Chapter IV)

   "Moderate Molecular Recognitions on ZnO m-Plane and Their Selective Capture/Release of Bio-related Phosphoric Acids"

   E. Kanao, K. Nakano, **R. Kamei**, T. Hosomi, Y. Ishihama, J. Adachi, T. Kubo, K. Otsuka and T. Yanagida

   ***Nanoscale Adv.,* 4**, 1649–1658 (2022)

3. (Chapter V)

   "Rational Strategy for Space-Confined Atomic Layer Deposition"

   R. Kamei, T. Hosomi, M. Kanai, E. Kanao, J. Liu, T. Takahashi, W. Li, W. Tanaka, K. Nagashima, K. Nakano, K. Otsuka, T. Kubo and T. Yanagida

   Submitted (under peer review)

International Conferences

R. Kamei, T. Hosomi, M. Kanai, E. Kanao, K. Nagashima, T. Takahashi, W. Tanaka, T. Kubo and T. Yanagida, "Space-Confined Atomic Layer Deposition," International Symposium on "Functionalization and Flexible Device Application of Atomic Scale Organic and Inorganic Material"Hokkaido, Japan, 2022/12/7-9. (Poster)

Domestic Conferences

亀井 龍真, 細見 拓郎, 金尾 英佑, 金井 真樹, 長島 一樹, 高橋 綱己, 張 国柱, 安井 隆雄, 寺尾 潤, 大塚 浩二, 久保 拓也, 柳田 剛,「メートル長のマイクロチューブにおける限られた空間での ZnO ナノワイヤのシード成長の合理的戦略」, 第 68 回応用物理学会春季学術講演会, オンライン開催, 17p-Z18-8, 2019 年 3 月 16-19 日.（口頭発表）

亀井 龍真, 金井 真樹, 細見 拓郎, 長島 一樹, 高橋 綱己, 張 国柱, 柳田 剛,「ZnO ナノワイヤを吸着層として利用する分子認識キャピラリーカラムの開発」, 第 5 回ナノ分析化学討論会, 愛媛大学　城北キャンパス, 愛媛, 2019 年 12 月 10,11 日.（口頭発表）